Table 1. List of the miRNAs That Are Predicted to Target Mouse Dnmt1 and Their Respective Expression in the MFH Model (miRNA Microarray Data)

	1-MFH_D2			2-MFH_D4			3-MFH_D6			4-MFH_D8			5-MFH_D10		
	Raw Data	Log2 (Raw Data)	Log2 (sample/MFHD2)	Raw Data	Log2 (Raw Data)	Log2 (Sample/MFHD2)	Raw Data	Log2 (Raw Data)	Log2 (Sample/MFHD2)	Raw Data	Log2 (Raw Data)	Log2 (Sample/MFHD2)	Raw Data	Log2 (Raw Data)	Log2 (Sample/MFDH2)
mmu-miR-128-3p	20.24	4.34	1.00	20.55	4.36	1.01	27.63	4.79	1.10	29.01	4.86	1.12	36.18	5.18	1.19
mmu-miR-130a-3p	1,536.74	10.59	1.00	1,962.51	10.94	1.03	2,443.93	11.25	1.06	2,425.60	11.24	1.06	2,721.55	11.41	1.08
mmu-miR-130b-3p	103.95	6.70	1.00	106.84	6.74	1.01	111.44	6.80	1.01	100.15	6.65	0.99	111.61	6.80	1.02
mmu-miR-148a-3p	90.36	6.50	1.00	180.16	7.49	1.15	407.07	8.67	1.33	476.92	8.90	1.37	527.02	9.04	1.39
mmu-miR-148b-3p	49.51	5.63	1.00	74.49	6.22	1.10	110.86	6.79	1.21	114.13	6.83	1.21	133.33	7.06	1.25
mmu-miR-152-3p	18.54	4.21	1.00	58.77	5.88	1.40	120.96	6.92	1.64	134.04	7.07	1.68	207.02	7.69	1.83
mmu-miR-301a-3p	395.46	8.63	1.00	353.92	8.47	0.98	387.68	8.60	1.00	359.38	8.49	0.98	380.23	8.57	0.99
mmu-miR-301b-3p	13.26	3.73	1.00	10.48	3.39	0.91	10.85	3.44	0.92	10.78	3.43	0.92	10.89	3.45	0.92
mmu-miR-326-3p	1.00	0	0	17.29	4.11	0	23.84	4.58	0	25.06	4.65	0	35.23	5.14	0
mmu-miR-330-3p	1.00	0	0	1.00	0	0	1.00	0	0	1.00	0	0	1.00	0	0
mmu-miR-495-3p	281.06	8.13	1.00	521.99	9.03	1.11	554.68	9.12	1.12	384.00	8.58	1.06	368.08	8.52	1.05
mmu-miR-1192	1.00	0	0	1.00	0	0	1.00	0	0	1.00	0	0	1.00	0	0

miR-148a in both rodent and human species (Fig. 4B). The miRNA prediction databases that we interrogated identified Dnmt1 as a high-scoring predicted target of

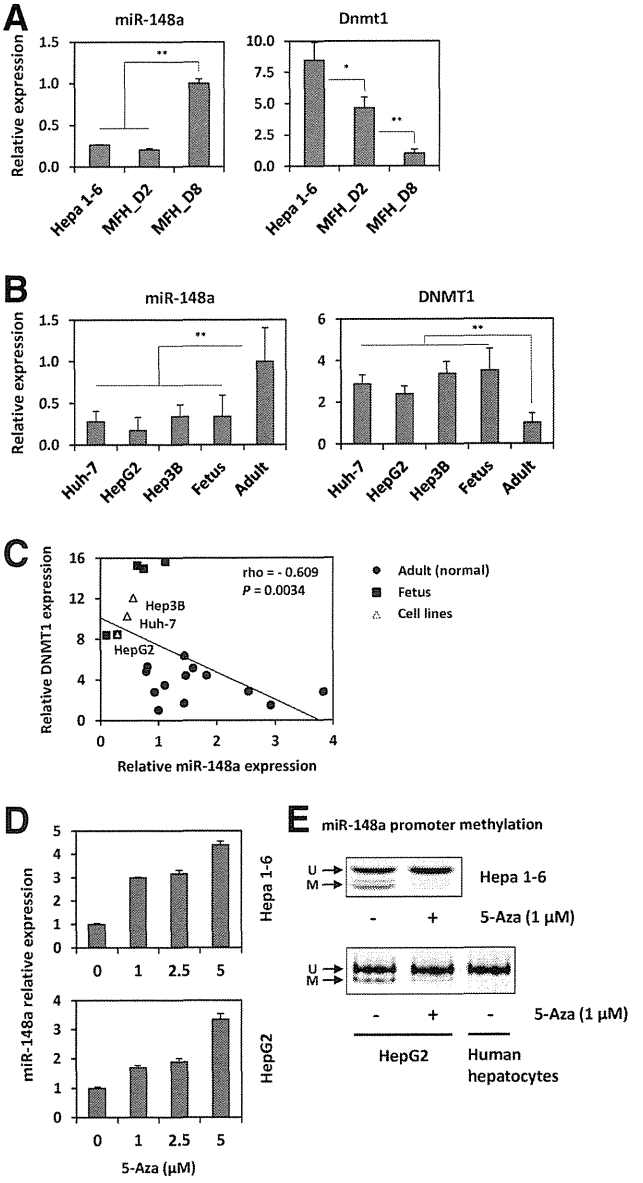

Fig. 3. miR-148a and Dnmt1 assessment in the liver. (A) The mouse hepatoma cell line, Hepa 1-6, was used to assess miR-148a and Dnmt1 mRNA levels, compared to undifferentiated hepatic stem cells (MFH D2) and mature-induced hepatocytes (MFH D8). (B) miR-148a and human DNMT1 expression were analyzed in the human HCC cell lines, Huh-7, HepG2, and Hep3B, and compared to a cohort of 13 normal livers as well as five lots of fetal livers. (C) Scatter plots of Spearman's correlation coefficient analysis between relative DNMT1 expression level and miR-148a. (D) Relative expression of miR-148a in Hepa 1-6 and HepG2 cells after 5 days of exposure to the hypomethylation agent, 5-Aza at 1, 2.5, and 5 μM. (E) COBRA of miR-148a promoter in Hepa 1-6 and HepG2 cells treated with or without 5-Aza for 5 days. Methylation status of the miR-148a promoter was also assessed in normal human hepatocytes. U, unmethylated; M, methylated. Statistical significance, compared to controls, was: $*P < 0.05$ and $**P < 0.01$ (t test) for RT-qPCR analysis.

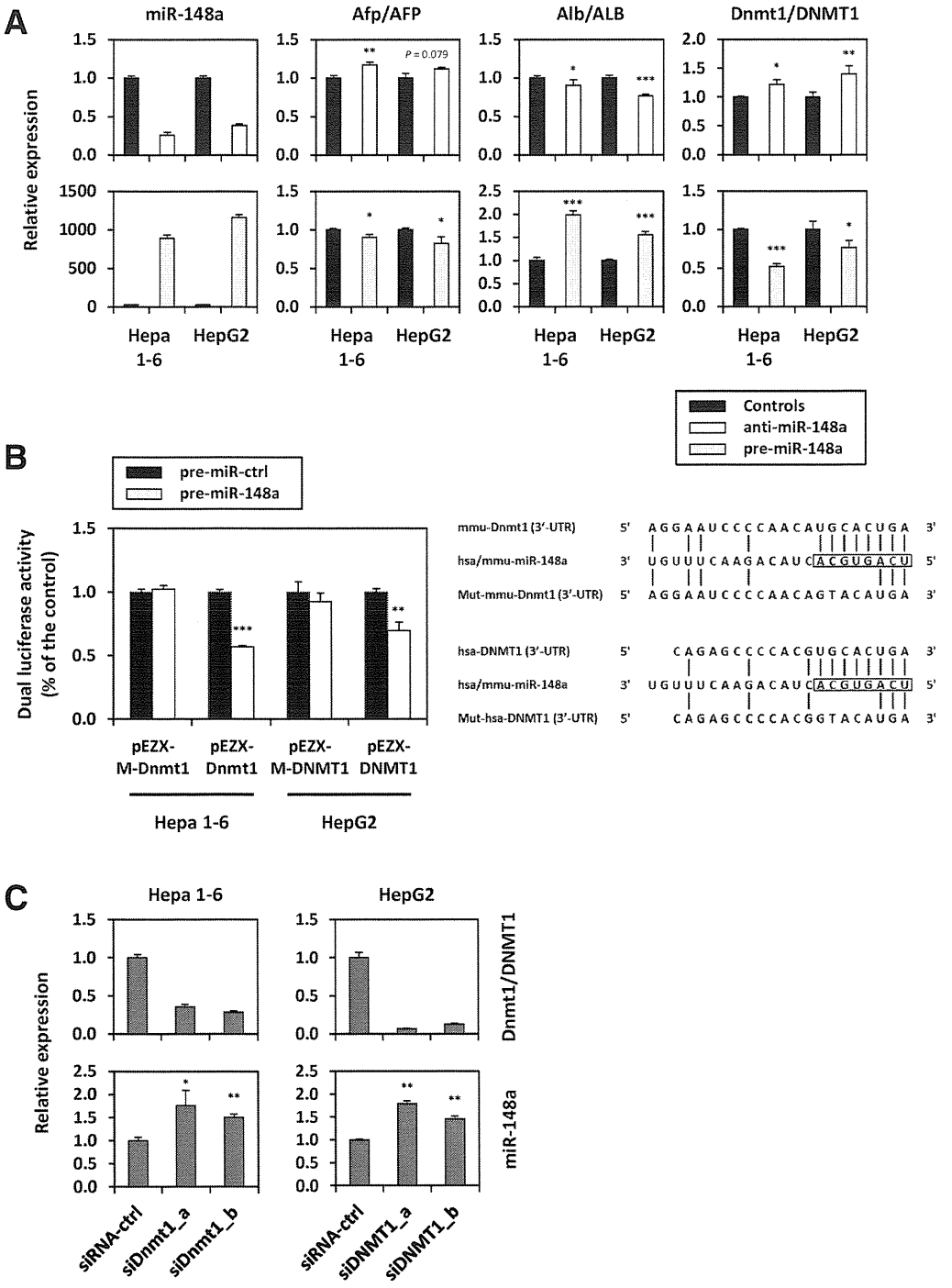

Fig. 4. Characterization of the relationship between miR-148a and DNMT1 in rodent and human models. (A) Relative expression of Dnmt1 and liver markers Afp and Alb, respectively, after experimental modulation of miR-148a in mouse Hepa 1-6 and human HepG2 cell lines. Cells were transfected using 100 ng of miR-148a mimics (pre-miR-148a) or antagonists (anti-miR-148a). Scramble miRNA mimics or antagonists were used as negative controls. Total RNAs were collected 72 hours post-transfection, and mRNA relative expression levels were determined by RT-qPCR. (B) Dual luciferase assay on Hepa 1-6 and HepG2 cells cotransfected with miR-148a mimics and the firefly/Renilla luciferase construct containing the mouse Dnmt1 or human DNMT1 3'-UTR. Mutated 3'-UTR sequences were used as negative controls, and ratios of firefly/Renilla luciferase activities were determined. Sequences indicate interaction sites between miR-148a and 3'-UTRs of mouse Dnmt1 and human DNMT1. (C) Transfection of Hepa 1-6 and HepG2 cells with siRNAs against mouse Dnmt1 and human DNMT1. Scramble siRNAs were used as negative controls (siRNA-ctrl). Total RNAs were used to analyze miR-148a expression by RT-qPCR 48 hours after transfection. Statistical significance: $*P < 0.05$; $**P < 0.01$; $***P < 0.001$ (*t* test).

miR-148a. Simultaneous transfection with miRNA mimics and a construct containing the mouse Dnmt1 3'-UTR inserted downstream of the luciferase coding sequence was performed in Hepa 1-6 cells. In this assay, miR-148a-forced expression decreased luciferase activity by 43.2% ± 1.1% ($P < 0.001$) from the control value,

whereas it failed to inhibit reporter activity in cells transfected with the vector containing a mutated sequence of the Dnmt1 3'-UTR (Fig. 4B). Comparable data were obtained using the 3'-UTR of human DNMT1 transfected into the human HCC cell line, HepG2. Then, to explore the role of DNMT1 in regulating expression of miR-148a, we silenced DNMT1 by using a siRNA approach in Hepa 1-6 and HepG2 cells. Both mouse Dnmt1 knockdown and human DNMT1 knockdown significantly induced miR-148a expression (Fig. 4C), reinforcing the idea of a regulatory circuit between DNMT1 and miR-148a as well as the existence of epigenetic regulation exerted by DNMT1 on miR-148a.

miR-148a Enhancement Promotes Hepatospecific Gene Expression Through Dnmt1 Inhibition During the Induced Differentiation of MFHs Into Mature Hepatocytes. The influence of miR-148a in hepatic differentiation was investigated by forcing its expression in the MFH primary culture model and evaluating the expression of major liver markers. Cells transfected with miR-148a mimics exhibited substantial overexpression of miR-148a, in contrast to its normal expression profile during MFH differentiation (Fig. 5A). Immunoblotting revealed that miR-148a overexpression dramatically increased the protein level of Alb in MFHs (Fig. 5B). The methylation status of the Alb promoter was also explored, which showed a progressive demethylation of CpG islands during hepatic differentiation (Supporting Fig. 3). Both 5-Aza treatment and miR-148a mimics contributed to the demethylation of Alb promoter, indicating the possible regulation of Alb expression by miR-148a through an epigenetic mechanism involving Dnmt1. RT-qPCR analysis demonstrated that miR-148a mimics enhanced the mRNA levels of Alb as well as the other major hepatic biomarkers, G6pc and Tat, whereas cells transfected by the control showed the standard differentiation process induced by the hepatotrophic factors (Fig. 5C). Moreover, miR-148a augmentation had no effect on Ck19 expression in MFHs, but it was associated with the increased expression of various CYPs (Supporting Fig. 4). Remarkably, we found evidence that miR-148a restoration in both mouse Hepa 1-6 and human HepG2 HCC cell lines was significantly related with the inhibition of the immature liver marker, Afp, whereas Alb expression was strongly enhanced, and *vice versa* (Fig. 4A). Last, the forced expression of miR-148a was correlated with a drastic repression of Dnmt1 in both the HCC (Fig. 4A) and MFH models (Fig. 5C). Western blotting analysis confirmed the negative correlation between miR-148a and DNMT1 expression levels (Fig. 5B). Indeed, the transfection of MFHs using miR-148a mimics promoted the decline of Dnmt1 that is normally observed during the differentiation process of these cells. To address the involvement of Dnmt1 in the establishment of the hepatic phenotype through its modulation by miR-148a, we finally analyzed the effect of Dnmt1 knockdown in the induced differentiation of MFHs. Consistent with miR-148a overexpression data, Dnmt1 inhibition led to the significant promotion of the major hepatic biomarkers that we assessed (Fig. 5D). Compared with MFHs transfected with negative control siRNAs, mRNA levels of Alb and advanced maturation biomarkers (G6pc, Tat, and Cyp17a1) appeared to be globally up-regulated 72 hours after Dnmt1 siRNA transfection.

In summary, these findings implicate Dnmt1 in the mechanisms controlling liver precursor maturation and indicate that miR-148a promotes the expression of adult hepatic genes by repressing Dnmt1 (Fig. 5E). In contrast, the occurrence of HCC malignancy may be associated with the deregulation of miR-148a, whereas maintenance of this miRNA seems to be essential for preserving the hepatospecific status of liver cells.

miR-148a Expression Is Frequently Decreased in the Liver of HCC Patients. We analyzed miR-148a expression in a cohort of 39 pairs of primary HCCs related to HBV or HCV infection and their adjacent nontumor regions. Tissues from normal liver (n = 13) were used as controls. miR-148a expression was reduced by more than 5-fold in HCC biopsies, relative to the normal liver group (median, 0.293 and 1.674, respectively; $P < 0.0001$, Mann-Whitney's U test; Fig. 6A). Interestingly, miR-148a was also inhibited in peritumoral non-neoplastic tissues, but to a lesser extent (median, 0.403; $P < 0.001$). We confirmed the possible correlation between miR-148a inhibition and advancement of the underlying liver disease by analyzing the expression level of miR-148a between early (chronic hepatitis) and advanced (precirrhotic/cirrhotic) fibrosis in nontumor tissues (Fig. 6B). Expression of miR-148a was significantly decreased in the cirrhotic samples, compared to the chronic hepatitis liver group (median, 0.247 and 0.473, respectively; $P < 0.0001$, Mann-Whitney's U test). Then, DNMT1 levels between tumors and their adjacent tissues were evaluated (Fig. 6C). Although DNMT1 expression was significantly down-regulated in tumors ($P = 0.0002$, Wilcoxon's signed-rank test), statistical analysis did not reveal significant correlation between DNMT1 and miR-148a expression in those clinical samples. Next, we compared the expression of miR-148a between

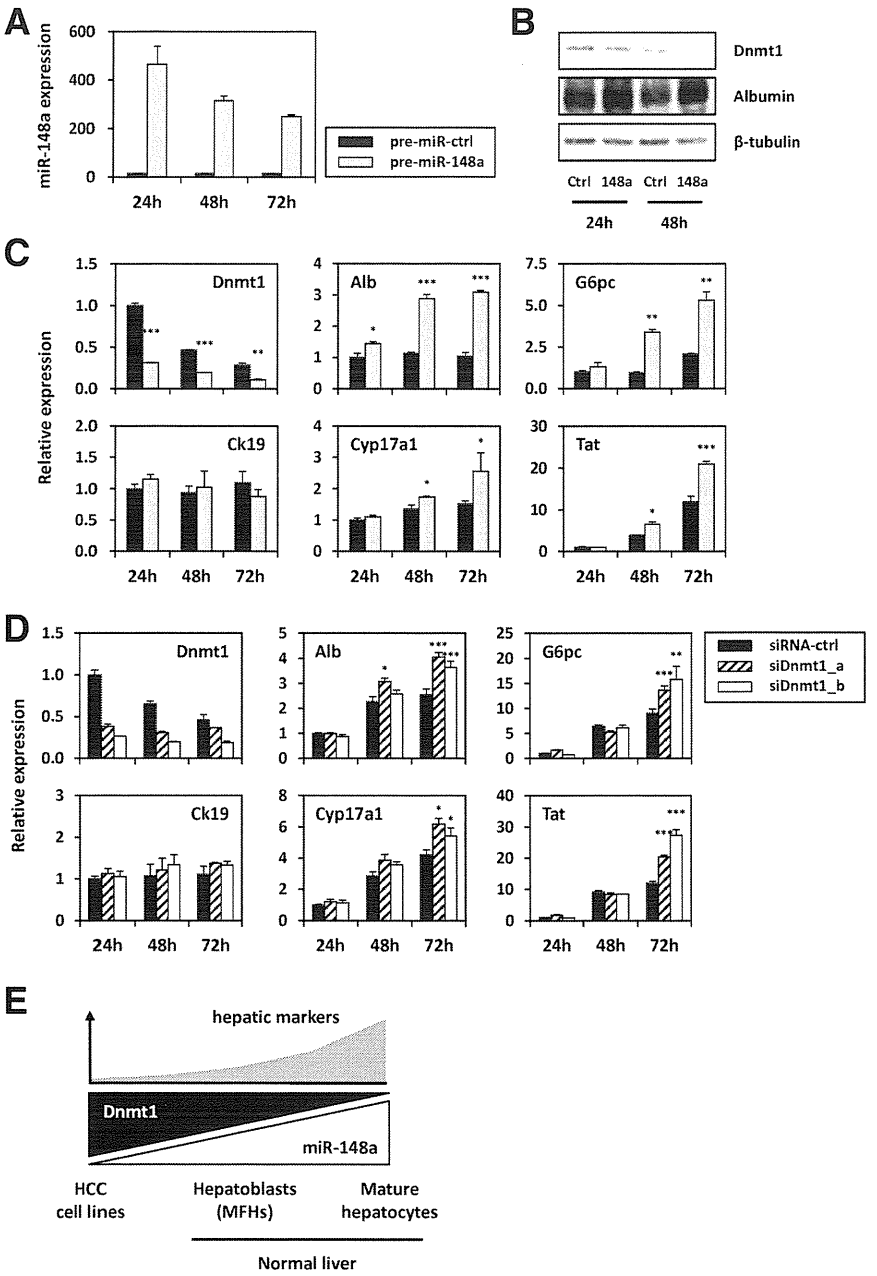

Fig. 5. Forcing expression of miR-148a promotes expression of hepatospecific genes during MFH-induced differentiation. MFH primary cultures were transfected using miR-148a mimics (100 nM) on the fourth day after cell isolation (MFH D4). Control miRNA mimics were used as negative controls. Total RNAs were extracted at the indicated times; then, miRNA and mRNA relative expression was determined by RT-qPCR. (A) MiR-148a overexpression in MFHs after transfection with miR-148a mimics (pre-miR-148a) or controls (pre-miR-ctrl). (B) Protein levels of Dnmt1 and Alb analyzed by immunoblotting 24 and 48 hours after MFH transfection by miR-148a mimics. β-tubulin was used as loading control. (C) Effect of miR-148a enforced induction on hepatic gene expression in the MFH model. mRNA levels of Alb and late hepatospecific makers (G6pc, Tat, and Cyp17a1) were analyzed. Dnmt1 and Ck19 were also evaluated in response to miR-148a overexpression. (D) Liver biomarker expression after Dnmt1 knockdown in MFHs. Transfections were performed the second day after cell sorting (MFH D2) using mouse Dnmt1 siRNAs, and RT-qPCR was performed at the indicated times. Statistical significance from control miRNAs and control siRNAs was reached at: $*P < 0.05$; $**P < 0.01$; $***P < 0.001$ (t test). (E) Schematic representation of the connection between miR-148a and Dnmt1 in the liver. During development, miR-148a expression is enhanced, inhibiting Dnmt1 and promoting induction of liver markers. In hepatic stem and HCC cells, miR-148a expression is repressed, leading to overexpression of Dnmt1 and silencing of hepatospecific genes.

tumors and their pair-matched normal tissues (Supporting Fig. 5). Of the 18 HBV-related HCC samples, miR-148a expression was decreased in 15 tumors, relative to their adjacent noncancerous hepatic regions ($P = 0.0268$, Wilcoxon's signed-rank test). In the 21 HCV-related HCCs, inhibition of miR-148a was observed in 12 HCC samples ($P = 0.9308$). The value of circulating miR-148a as a noninvasive HCC

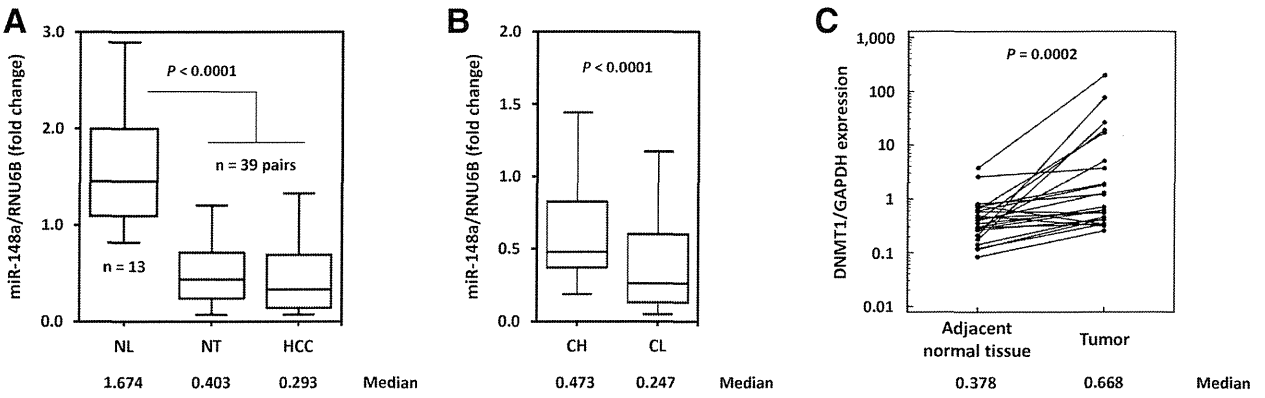

Fig. 6. Expression of miR-148a in liver clinical samples. (A) Plot boxes illustrating differential expression of miR-148a in 13 normal livers (NL), 39 primary HCCs (HCC), and their corresponding nontumor tissues (NT). Expression of miR-148a was normalized to RNU6B. Boxes show median and 25th and 75th percentiles, whereas vertical bars display the range of values. Within the box, 50% of values are shown, and 80% are included between the extremities of vertical bars. Mann-Whitney's U test indicated statistical underexpression of miR-148a in both HCC and adjacent NT tissues, compared to the normal liver group ($P < 0.0001$). (B) Expression of miR-148a in nontumor tissues between chronic hepatitis (CH) and precirrhotic/cirrhotic livers (CL). Statistical analyses showed significant inhibition in the CL group ($P < 0.0001$, Mann-Whitney's U test). (C) Comparison of DNMT1 expression levels between primary tumor and peritumoral non-neoplastic tissue from 24 randomly selected pairs. Statistical differences were analyzed with Wilcoxon's signed-rank test and indicated significant overexpression in tumor versus the normal group ($P = 0.0002$).

recurrence diagnostic marker in blood serum was also evaluated. Samples were collected in two steps from 11 HCC patients with HCV infection: (1) after surgical resection of the primary tumor and (2) subsequent to the diagnosis of HCC recurrence. We observed a diminution of circulating miR-148a in 8 patients after HCC recurrence ($P = 0.2783$, Wilcoxon's signed-rank test; Supporting Fig. 6).

The Rescue of miR-148a Suppresses HCC Cell Migration and Invasion by Indirectly Inhibiting the Hepatocyte Growth Factor Receptor Oncogene. As we highlighted the crucial role played by miR-148a in normal hepatic differentiation, it was of significant interest to consider the possible relationship between miR-148a deregulation and the promotion of hepatocyte transformation. First, the phenotype of Hepa 1-6 cells was characterized after the forced expression of miR-148a to investigate the effect of this miRNA on HCC cells. Notably, cell proliferation was not significantly altered by miR-148a mimics or antagonists (Fig. 7A), and induction of miR-148a had no effect on caspase activity (Supporting Fig. 7). However, the enforced expression of miR-148a substantially suppressed the motility of HCC cells in a wound-healing assay, whereas miR-148a agonists enhanced the recolonization of the wounds (Fig. 7B). In addition, overexpression of miR-148a remarkably altered the invasive abilities of Hepa 1-6 cells ($51.6\% \pm 10.15\%$ inhibition; $P < 0.001$), as revealed by the transwell migration assay (Fig. 7C). A similar observation was conducted using the human HCC cell line, Hep3B (data not shown). To evaluate whether the effect of miR-148a in the invasion of HCC cells is mediated by DNMT1 or another specific gene, functional analyses were performed using siRNA. We decided to focus on DNMT1 and hepatocyte growth factor receptor (c-Met), a frequently overexpressed oncogene in liver cancer and predicted target of miR-148a that was up-regulated in undifferentiated MFHs and Hepa 1-6 HCC cells (Supporting Fig. 8). In the presence of miR-148a mimics, c-Met mRNA levels appeared markedly decreased in Hepa 1-6, whereas miR-148a agonists promoted c-Met expression (Fig. 7D). However, c-Met 3'-UTR assays did not show a reduction of luciferase activity (Supporting Fig. 8), supporting an indirect effect of miR-148a on c-Met expression. Knockdown of c-Met using two distinct siRNAs attenuated cell proliferation (Fig. 7E) and dramatically abolished HCC cell invasion ($78.8\% \pm 7.7\%$ and $76.5\% \pm 7.5\%$ inhibition, respectively; $P < 0.001$; Fig. 7F). Remarkably, the use of siRNAs targeting Dnmt1 did not modify cell proliferation or invasion. These last results strongly suggest that miR-148a plays two distinct roles in the liver: (1) in the control of hepatic development by regulating DNMT1 and (2) in the modulation of HCC cell invasiveness by repressing the c-Met oncogene.

Discussion

DNA methylation plays an essential role in regulating stem cell differentiation and embryo development. Recently, Tsai et al. demonstrated that the pluripotency genes, *Oct4* and *Nanog*, which constitute a fundamental regulatory mechanism suppressing

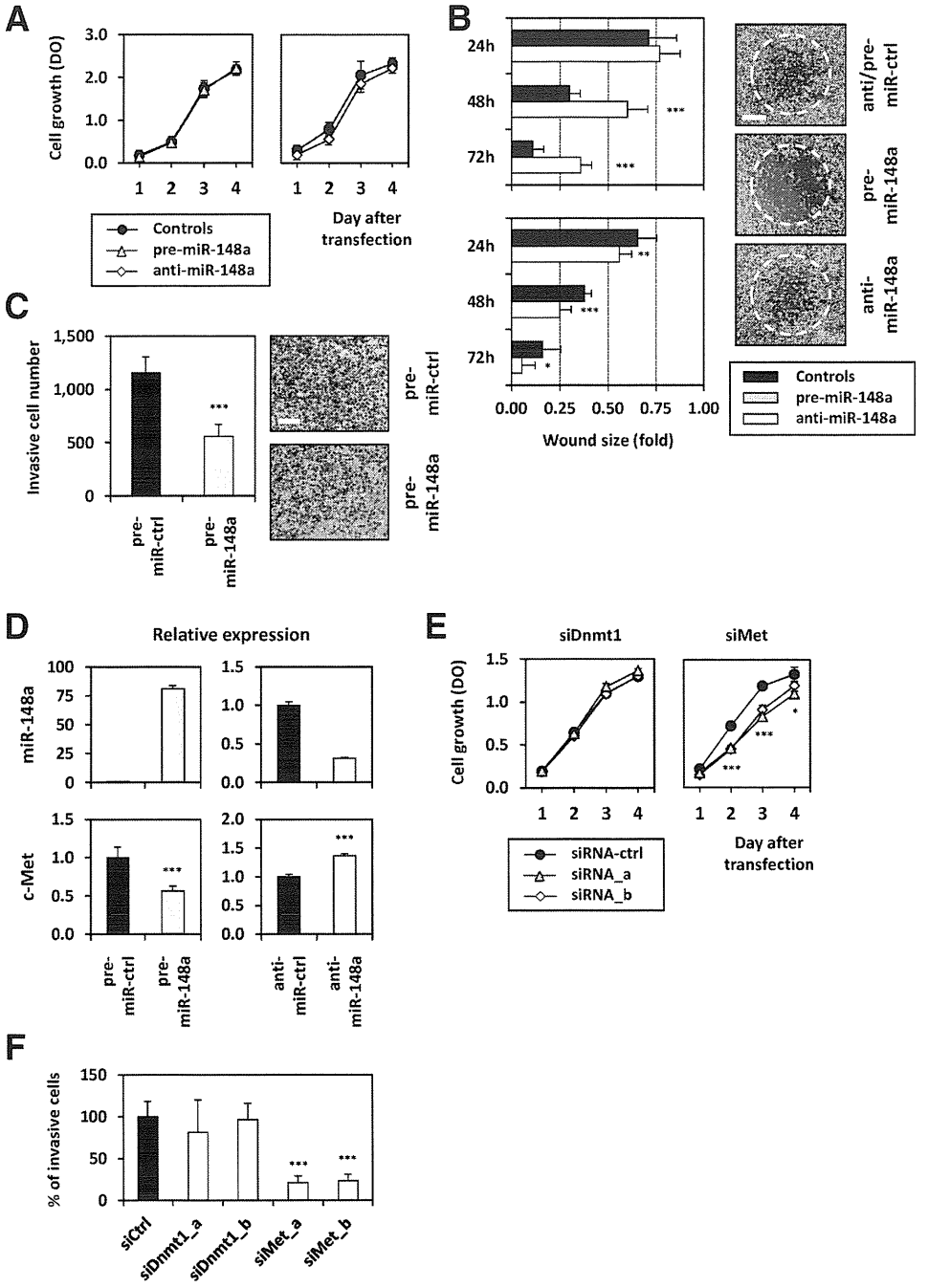

Fig. 7. Consequence of miR-148a rescue on HCC cell phenotype. (A) Hepa 1-6 cell growth determined at indicated times after miR-148a amplification or repression. No significant difference was found (*t* test). (B) Hepa 1-6 migratory abilities after miR-148a overexpression or inhibition in the presence of HGF (50 ng/mL). Cell monolayers were wounded 24 hours after transfection, and the sizes of the wounds were measured at indicated times. Bar: 500 μm. (C) Effect of miR-148a overexpression on cellular invasion ability. FBS (10%) and HGF (100 ng/mL) were used as chemoattractants for transwell invasion assays. Bar: 250 μm. (D) Expression of c-Met oncogene 48 hours after Hepa 1-6 transfection with miR-148a mimics or antagonists. (E) Assessment of Hepa 1-6 proliferation and (F) invasion ability after Dnmt1 and c-Met knockdown by using two distinct siRNAs for each. Statistical significance, compared to controls: $*P < 0.05$; $**P < 0.01$; $***P < 0.001$ (*t* test).

differentiation-associated genes, directly bind to the promoter of DNMT1 and enhance its expression.[21] In their report, mesenchymal stem cells exhibited a decreased proliferation rate when treated with an inhibitor of DNA methylation or transfected with DNMT1 short hairpin RNA, whereas the expression of genes associated with development regulators was increased. In agreement with this current work, our data clearly show the contribution of the DNMT1 enzyme in liver cell stemness as well as the existence of a micromanagement of DNMT1-related hepatic maturation controlled by miR-148a.

The deleterious consequences of DICER-silencing experiments in mouse embryonic stem cells demonstrated that miRNA processing plays a major role in development.[22] In the liver, Sekine et al. tested the consequence of DICER1 silencing by performing conditional knockout in hepatocytes.[23] Remarkably, hepatocytes exhibiting DICER1-specific depletion displayed a gene expression profile indicative of cell growth and dedifferentiation into liver progenitors. Although the role of miRNAs in cell specification has been addressed in a number of tissues,[6,24] little is known regarding the involvement of specific miRNAs in the control of hepatic development. miR-122 is probably an essential actor in liver ontogenesis, as suggested by its remarkable expression in the adult liver and its ability to induce CYPs in HCC cell lines.[25] The case of miR-148a also appears of prime interest in cell lineage determination, as previously described in hematopoietic stem cell specification[26] and myogenic differentiation.[27] In the last case, Zhang et al. showed the positive role of miR-148a in skeletal muscle development by the translational repression of ROCK1, an inhibitor of myogenesis.

Consistent with our results, other studies have demonstrated that miRNAs can control expression of DNMTs. In the liver, miR-140 can target the 3'-UTR of DNMT1 and control nuclear factor kappa B activity.[28] In addition, some splicing isoforms of DNMT3b have been found to be directly repressed by miR-148a.[29] Conversely, epigenetic mechanisms are considered essential for miRNA regulation.[30] The genomic sequence of miR-148a has been analyzed in a number of cancer cell lines with distinct tissue origins, as well as a large amount of CpG islands found in its promoter region. Thus, inactivation of miR-148a by DNA hypermethylation and DNMT1 overexpression has recently been demonstrated in pancreatic,[31] gastric,[32] and breast cancer.[33] Consequently, the network of feedback between miRNAs and epigenetic pathways appears to form a complex regulatory system that is essential to organize gene expression profile and maintain cell integrity. miR-148a and DNMT1 certainly constitute a regulatory circuit that is disrupted in HCC tissues. On the one hand, overexpression of DNMT1 leads to hypermethylation of the promoter region of miR-148a, causing its silencing. On the other hand, miR-148a alteration reduces its silencing action on DNMT1, resulting in augmentation of DNMT1 expression and maintaining hypermethylation of the miR-148a promoter.

Our data finally suggest that miR-148a restoration may provide a valuable strategy for therapeutic applications by inhibiting c-Met expression and repressing HCC cell invasion. Pertinent studies previously indicated that the use of miRNA precursors could contribute to the development of promising miRNA-based therapeutic methods. For instance, Kota et al. showed that systemic administration of miR-26a in rodents led to a remarkable slowdown of HCC progression without toxicity.[34] These observations suggest that the delivery of tumor-suppressor–type miRNAs, such as miR-148a and miR-122, which are highly expressed and therefore well tolerated in normal adult tissues, but lost in transformed cells, may provide a general strategy for miRNA replacement therapies. miR-148a also represents a valuable marker for the diagnosis and prognosis of HCC because its expression is frequently inhibited in liver cancer. Our observation that miR-148a alteration is not limited to the tumor site, but also affects the peritumoral nonneoplastic tissue, is noteworthy. This down-regulation is probably the consequence of the chronic inflammatory context inherent to hepatitis virus infection and liver fibrosis, which could represent an early event in CLDs, leading to augmentation of DNMT1 activity and aberrant DNA methylation. In this regard, Braconi et al. reported that the inflammation-associated cytokine, interleukin-6, regulates DNMT1 activity and methylation-dependent tumor-suppressor genes by modulating miR-148a/152 family expression in malignant cholangiocytes.[35] Furthermore, another study showed that miR-152 is frequently down-regulated in HBV-related HCC, inducing DNMT1 augmentation and aberrant DNA methylation.[36]

To conclude, our study demonstrates the existence of a dual role played by miR-148a in the liver. Importantly, we highlight a novel miRNA-mediated regulation mechanism in which miR-148a positively regulates hepatic differentiation by repressing DNMT1 expression. To our knowledge, this report is the first to demonstrate an effective promotion of the hepatospecific phenotype by modulating the expression of a single specific miRNA in a primary culture model using liver stem cells.

Acknowledgement: The authors thank A. Inoue, who offered excellent technical support throughout this study. The authors are also grateful to M. Kawamata, F. Takeshita, Y. Yoshioka, and T. Katsuda for their constructive comments on this work.

References

1. Ambros V. The functions of animal microRNAs. Nature 2004; 431:350-355.

2. Bartel DP. MicroRNAs: genomics, biogenesis, mechanism, and function. Cell 2004;116:281-297.
3. Calin GA, Croce CM. MicroRNA signatures in human cancers. Nat Rev Cancer 2006;6:857-866.
4. Gailhouste L, Ochiya T. Cancer-related microRNAs and their role as tumor suppressors and oncogenes in hepatocellular carcinoma. Histol Histopathol 2013;28:437-451.
5. Gailhouste L, Gómez-Santos L, Ochiya T. Potential applications of miRNAs as diagnostic and prognostic markers in liver cancer. Front Biosci 2013;18:199-223.
6. Gangaraju VK, Lin H. MicroRNAs: key regulators of stem cells. Nat Rev Mol Cell Biol 2009;10:116-125.
7. Cheng LC, Pastrana E, Tavazoie M, Doetsch F. miR-124 regulates adult neurogenesis in the subventricular zone stem cell niche. Nat Neurosci 2009;12:399-408.
8. Zhao C, Sun G, Li S, Shi Y. A feedback regulatory loop involving microRNA-9 and nuclear receptor TLX in neural stem cell fate determination. Nat Struct Mol Biol 2009;16:365-371.
9. Crist CG, Montarras D, Pallafacchina G, Rocancourt D, Cumano A, Conway SJ, et al. Muscle stem cell behavior is modified by microRNA-27 regulation of Pax3 expression. Proc Natl Acad Sci U S A 2009;106: 13383-13387.
10. Hand NJ, Master ZR, Eauclaire SF, Weinblatt DE, Matthews RP, Friedman JR. The microRNA-30 family is required for vertebrate hepatobiliary development. Gastroenterology 2009;136:1081-1090.
11. Girard M, Jacquemin E, Munnich A, Lyonnet S, Henrion-Caude A. miR-122, a paradigm for the role of microRNAs in the liver. J Hepatol 2008;48:648-656.
12. Li E. Chromatin modification and epigenetic reprogramming in mammalian development. Nat Rev Genet 2002;3:662-673.
13. Hermann A, Gowher H, Jeltsch A. Biochemistry and biology of mammalian DNA methyltransferases. Cell Mol Life Sci 2004;61:2571-2587.
14. Okano M, Bell DW, Haber DA, Li E. DNA methyltransferases Dnmt3a and Dnmt3b are essential for de novo methylation and mammalian development. Cell 1999;99:247-257.
15. Chan MF, van Amerongen R, Nijjar T, Cuppen E, Jones PA, Laird PW. Reduced rates of gene loss, gene silencing, and gene mutation in Dnmt1-deficient embryonic stem cells. Mol Cell Biol 2001;21:7587-7600.
16. Lei H, Oh SP, Okano M, Juttermann R, Goss KA, Jaenisch R, et al. De novo DNA cytosine methyltransferase activities in mouse embryonic stem cells. Development 1996;122:3195-3205.
17. Sen GL, Reuter JA, Webster DE, Zhu L, Khavari PA. DNMT1 maintains progenitor function in self-renewing somatic tissue. Nature 2010; 463:563-567.
18. Saito Y, Kanai Y, Sakamoto M, Saito H, Ishii H, Hirohashi S. Expression of mRNA for DNA methyltransferases and methyl-CpG-binding proteins and DNA methylation status on CpG islands and pericentromeric satellite regions during human hepatocarcinogenesis. HEPATOLOGY 2001;33:561-568.
19. Saito Y, Kanai Y, Nakagawa T, Sakamoto M, Saito H, Ishii H, et al. Increased protein expression of DNA methyltransferase (DNMT) 1 is significantly correlated with the malignant potential and poor prognosis of human hepatocellular carcinomas. Int J Cancer 2003;105: 527-532.
20. Gailhouste L. Isolation and purification method of mouse fetal hepatoblasts. Methods Mol Biol 2012;826:33-47.
21. Tsai CC, Su PF, Huang YF, Yew TL, Hung SC. Oct4 and Nanog directly regulate Dnmt1 to maintain self-renewal and undifferentiated state in mesenchymal stem cells. Mol Cell 2012;47:169-182.
22. Bernstein E, Kim SY, Carmell MA, Murchison EP, Alcorn H, Li MZ, et al. Dicer is essential for mouse development. Nat Genet 2003;35: 215-217.
23. Sekine S, Ogawa R, Ito R, Hiraoka N, McManus MT, Kanai Y, et al. Disruption of Dicer1 induces dysregulated fetal gene expression and promotes hepatocarcinogenesis. Gastroenterology 2009;136:2304-2315.e1-4.
24. Sayed D, Abdellatif M. MicroRNAs in development and disease. Physiol Rev 2011;91:827-887.
25. Xu H, He JH, Xiao ZD, Zhang QQ, Chen YQ, Zhou H, et al. Liver-enriched transcription factors regulate microRNA-122 that targets CUTL1 during liver development. HEPATOLOGY 2010;52:1431-1442.
26. Merkerova M, Vasikova A, Belickova M, Bruchova H. MicroRNA expression profiles in umbilical cord blood cell lineages. Stem Cells Dev 2010;19:17-26.
27. Zhang J, Ying ZZ, Tang ZL, Long LQ, Li K. MicroRNA-148a promotes myogenic differentiation by targeting the ROCK1 gene. J Biol Chem 2012;287:21093-21101.
28. Takata A, Otsuka M, Yoshikawa T, Kishikawa T, Hikiba Y, Obi S, et al. MiRNA-140 acts as a liver tumor suppressor by controlling NF-kappaB activity via directly targeting Dnmt1 expression. HEPATOLOGY 2013;57:162-170.
29. Duursma AM, Kedde M, Schrier M, le Sage C, Agami R. miR-148 targets human DNMT3b protein coding region. RNA 2008;14:872-877.
30. Sato F, Tsuchiya S, Meltzer SJ, Shimizu K. MicroRNAs and epigenetics. FEBS J 2011;278:1598-1609.
31. Hanoun N, Delpu Y, Suriawinata AA, Bournet B, Bureau C, Selves J, et al. The silencing of microRNA 148a production by DNA hypermethylation is an early event in pancreatic carcinogenesis. Clin Chem 2010;56:1107-1118.
32. Zhu A, Xia J, Zuo J, Jin S, Zhou H, Yao L, et al. MicroRNA-148a is silenced by hypermethylation and interacts with DNA methyltransferase 1 in gastric cancer. Med Oncol 2011.
33. Xu Q, Jiang Y, Yin Y, Li Q, He J, Jing Y, et al. A regulatory circuit of miR-148a/152 and DNMT1 in modulating cell transformation and tumor angiogenesis through IGF-IR and IRS1. J Mol Cell Biol 2013;5:3-13.
34. Kota J, Chivukula RR, O'Donnell KA, Wentzel EA, Montgomery CL, Hwang HW, et al. Therapeutic microRNA delivery suppresses tumorigenesis in a murine liver cancer model. Cell 2009;137:1005-1017.
35. Braconi C, Huang N, Patel T. MicroRNA-dependent regulation of DNA methyltransferase-1 and tumor suppressor gene expression by interleukin-6 in human malignant cholangiocytes. HEPATOLOGY 2010;51:881-890.
36. Huang J, Wang Y, Guo Y, Sun S. Down-regulated microRNA-152 induces aberrant DNA methylation in hepatitis B virus-related hepatocellular carcinoma by targeting DNA methyltransferase 1. HEPATOLOGY 2010;52:60-70.

FEBS Letters 587 (2013) 2377–2384

FEBS Letters

journal homepage: www.FEBSLetters.org

Selective control of SNARE recycling by Golgi retention

Masayoshi Fukasawa [a], Anda Cornea [b], Oleg Varlamov [c,*]

[a] Department of Biochemistry and Cell Biology, National Institute of Infectious Diseases, Tokyo, Japan
[b] Imaging and Morphology Support Core, Oregon National Primate Research Center, Beaverton, OR 97006, United States
[c] Division of Diabetes, Obesity and Metabolism, Oregon National Primate Research Center, Beaverton, OR 97006, United States

ARTICLE INFO

Article history:
Received 6 March 2013
Revised 4 June 2013
Accepted 4 June 2013
Available online 20 June 2013

Edited by Felix Wieland

Keywords:
Golgi
SNARE
Recycling
Retention
Endoplasmic reticulum
ER
Lipid raft
Membrane fusion
Vesicle
Dynamic equilibrium
i-SNARE
Homotypic fusion
Golgi tether
Entropy

ABSTRACT

Two distinct sets of soluble *N*-ethylmaleimide-sensitive factor attachment protein receptors (SNARE) catalyze membrane fusion in the *cis*-Golgi and *trans*-Golgi. The mechanism that controls Golgi localization of SNAREs remains largely unknown. Here we tested three potential mechanisms, including vesicle recycling between the Golgi and the endoplasmic reticulum, partitioning in Golgi lipid microdomains, and selective intra-Golgi retention. Recycling rates showed a linear relationship with intra-Golgi mobility of SNAREs. The *cis*-Golgi SNAREs had higher mobility than intra-Golgi SNAREs, whereas vesicle SNAREs had higher mobility than target membrane SNAREs. The differences in SNARE mobility were not due to preferential partitioning into detergent-resistant membrane microdomains. We propose that intra-Golgi retention precludes entropy-driven redistribution of SNAREs to the endoplasmic reticulum and endocytic compartments.

1. Introduction

The Golgi apparatus is a polarized organelle that mediates protein transport between the endoplasmic reticulum (ER) and endocytic compartments. The *cis*-Golgi is a receiver of anterograde vesicles traveling from the ER, whereas the *trans*-Golgi is a departure site for vesicles traveling to endocytic compartments [1]. The ER resident proteins that escape to the Golgi and Golgi proteins cycle back to the ER via the retrograde pathway [2–9].

Soluble *N*-ethylmaleimide-sensitive factor attachment protein receptors (SNAREs) [10] play a fundamental role in membrane fusion and have a polarized, gradient-like distribution in the Golgi. The vesicle (*v*)-SNARE proteins rBet1 [11,12], and the target membrane (*t*)-SNAREs Ers24 (Sec22) [12,13], p27 (Gs27, membrin) [14,15] are enriched in the *cis*-Golgi, whereas the *t*-SNAREs Syntaxin5 (Sed5) [16,17], Gos28 (Gs28, p28, Gos1p) [18–20] and Ykt6 [21] and the *v*-SNARE Gs15 (Sft1) [21,22] are enriched intra-Golgi and in the *trans*-Golgi. Morphological and biochemical studies suggest that at least two SNARE complexes (SNAREpins), the *cis*-Golgi *v*-[rBet1]:*t*-[Ers24-p27-Syntaxin5] and the *trans*-Golgi *v*-[Gs15]:*t*-[Ykt6-Gos28-Syntaxin5], catalyze membrane fusion in the Golgi stack [15,23–26].

While the distribution of Golgi SNAREpins is well established, the mechanisms that control their distribution across the Golgi stack are largely unknown. Here we tested three potential mechanisms responsible for SNARE localization in the Golgi: vesicle-mediated recycling between the Golgi and the ER, selective partitioning in the Golgi membrane microdomains, and selective retention in the Golgi. Finally, we propose a new idea how fusogenic and inhibitory SNARE complexes [27] can generate SNARE gradients in the early secretory pathway.

* Corresponding author. Address: L584, Oregon National Primate Research Center, 505 NW 185th Ave. Beaverton, OR 97006, United States.
E-mail address: varlamov@ohsu.edu (O. Varlamov).

0014-5793/$36.00
http://dx.doi.org/10.1016/j.febslet.2013.06.004

2. Results

2.1. SNARE recycling between the Golgi and the ER

Protein recycling between the Golgi and the ER is mediated by anterograde and retrograde transport (Fig. 1C). We computed the rate of anterograde transport (K_{in}) and the rate of retrograde transport (K_{out}) for various SNARE proteins using fluorescence recovery after photobleaching (FRAP) [28]. The Golgi membrane SNARE proteins rBet1, Ers24, p27, Gos28, Syntaxin5 and Gs15 were tagged with the cyan fluorescent protein (CFP) and expressed in NRK cells as previously described [29]. K_{in} values were calculated from single-exponential fits of fluorescence recovery curves after photobleaching the Golgi (Fig. 1A and B and Supplementary videos), whereas K_{out} values were determined based on fluorescence recovery after photobleaching the ER (Fig. 3 and Supplementary videos).

For all SNARE proteins examined, K_{in} were not significantly different than the corresponding K_{out} values (Fig. 1D and 3B). K_{in} values for rBet1 were significantly higher than K_{in} values for all other SNARE proteins, but no statistically significant differences in K_{in} values were detected between any other combinations of SNAREs (Fig. 1D). To confirm that fluorescence recovery represents the vesicle-mediated transport step that originates in the ER, we treated digitonin-permeabilized cells with the dominant-negative mutant of GTPase Sar1T39N, the inhibitor of COPII vesicle formation at the ER exit sites [30,31]. To verify that fluorescence recovery in

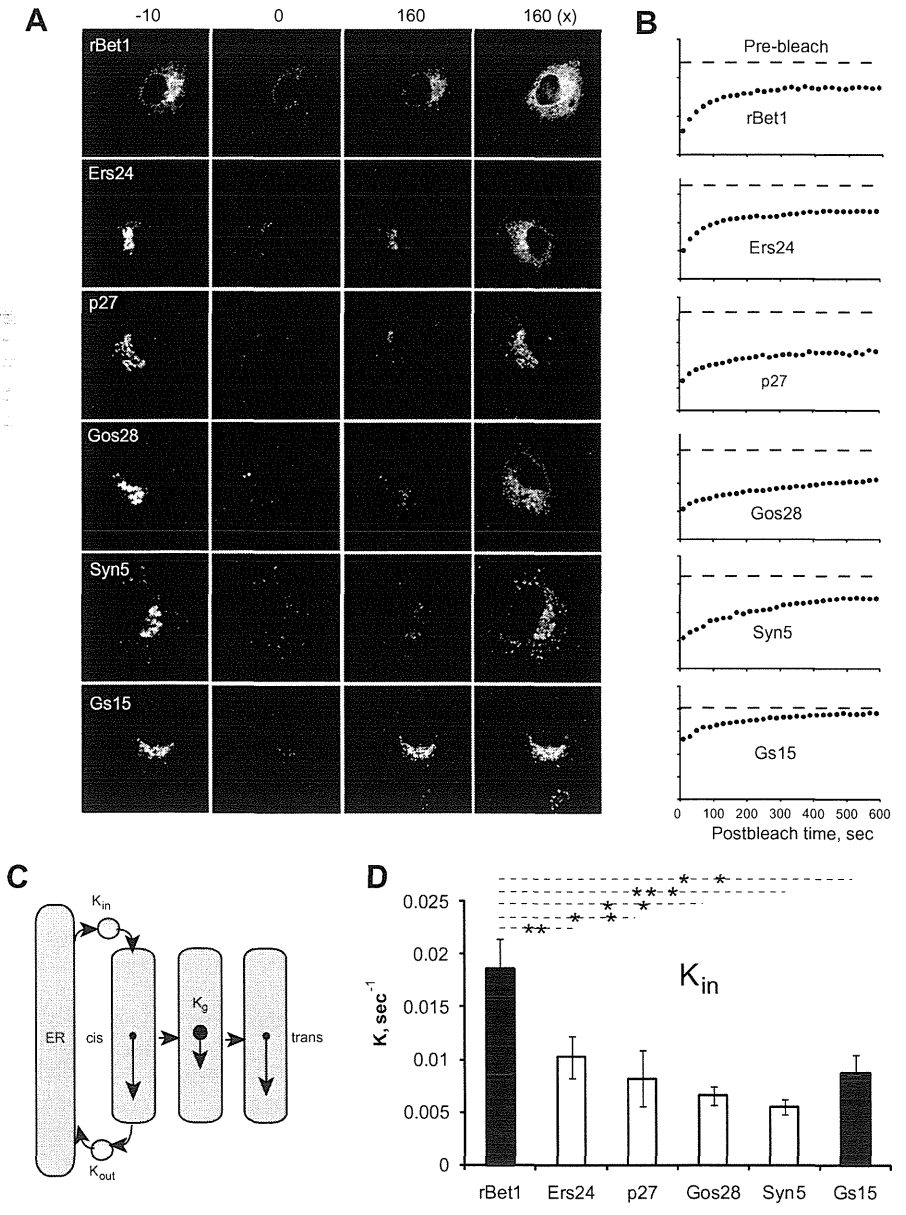

Fig. 1. Anterograde transport of SNARE proteins in the early secretory pathway. CFP-tagged Golgi SNARE proteins were transiently expressed in NRK cells, the Golgi regions were bleached, and anterograde transport rates were determined following fluorescence recovery in the Golgi. (A) Representative images showing the pre-bleaching (−10 s), the post-bleaching (0 s), and the post-recovery stages (160 s) of FRAP. The later set of images is shown at higher contrast (160×). Scale bar = 10 μm. (B) Representative fluorescence traces showing the kinetics of fluorescence recovery in the Golgi following photobleaching. The ordinate represents the arbitrary fluorescence units. (C) Protein recycling in the early secretory pathway. The ER and the Golgi are bound bi-directionally by anterograde transport (represented by the rate K_{in}) and by retrograde transport (represented by the rate K_{out}). Intra-Golgi rates (K_g) represent protein mobility in the Golgi membranes. (D) the Golgi. K_{in} values were calculated from single-exponential fits of fluorescence recovery curves after photobleaching the Golgi as described in Section 5. Bars are means ± S.E.M. for n = 10–15 cells. Statistically significant differences between K_{in} values were determined using One-way ANOVA; $^{**}P < 0.01$; $^{***}P < 0.001$

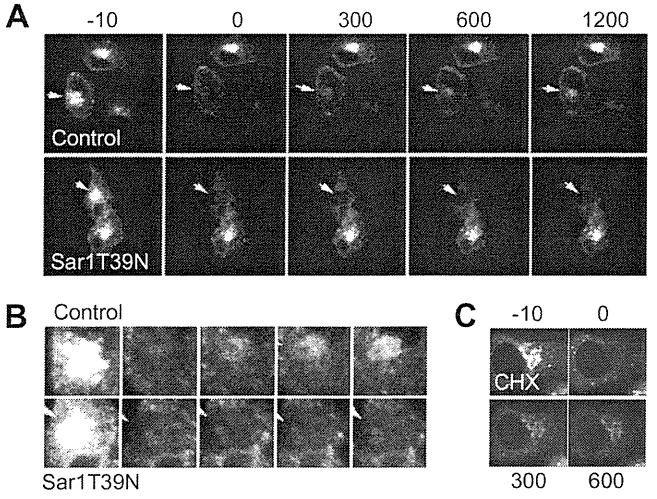

Fig. 2. Anterograde transport of SNAREs requires the ER exit sites. (A) Digitonin-permeabilized cells expressing CFP-GOS28 were incubated with transport mixture in the presence or absence of the dominant-negative mutant Sar1 T39 N. The Golgi regions of permeabilized cells (arrows) were photobleached, and the recovery of fluorescence in the Golgi was monitored as described above. (B) Enlarged image of the Golgi regions from "A". (C) Cells expressing CFP-GOS28 were pretreated for 2 h with 100 μg/ml cycloheximide and the recovery of fluorescence in the Golgi was monitored as described in Section 5.

the Golgi requires membrane fusion, we pretreated intact cells with the membrane fusion inhibitor *N*-ethylmaleimide. Anterograde transport was inhibited by *N*-ethylmaleimide (data not shown), and by Sar1T39N (Fig. 2A and B). Pretreatment of cells with the protein synthesis inhibitor cycloheximide did not alter anterograde transport (Fig. 2C).

K_{out} values for rBet1 were significantly higher than K_{out} values for Gos28, Syntaxin5 and Gs15, although no significant differences between K_{out} for rBet1 and K_{out} for Ers24 and p27 were detected (Fig. 3B). There was a strong linear correlation ($R^2 = 0.96$) between K_{in} and K_{out} values, consistent with the "*trans* < *cis*" distribution of Golgi SNARE proteins [15,23–26]: Syntaxin5 < Gos28 < p27 < Ers24 < rBet1 (Fig. 3C). Thus, the *cis*-Golgi SNAREs cycle at higher rates than intra-Golgi SNAREs. Gs15 was excluded from a linear regression analysis because its K_{in} was higher than what can be expected for the *trans*-Golgi SNARE (Fig. 3C).

2.2. Partitioning of SNARE proteins in membrane microdomains

Recent studies suggest that exocytic SNAREs are enriched in detergent-resistant lipid microdomains (lipid rafts) [32–36]. We thus tested whether Golgi SNARE proteins can also differentially partition into lipid microdomains in NRK and HELA cells. Cells were extracted with the cold non-ionic detergent Lubrol WX followed by sucrose density centrifugation (Supplementary Fig. 1S). Light fractions 3–5 on the sucrose density gradient represent detergent-resistant lipid domains, whereas the bottom fractions represent detergent-soluble lipid domains. Immunoblot analysis of gradient fractions revealed differential partitioning of endogenous secretory pathway proteins into detergent-resistant fractions (Fig. 4). Proteins that were highly enriched in detergent-resistant membranes included Caveolin-1 (plasma membrane, endosomes and TGN), SNAREs Vti1a, Vti1b and Syntaxin6 (endosomes and TGN), Rab6a (GTPase involved in *post*-Golgi and intra-Golgi transport), and TGN38 [37–39]. *Trans*-Golgi SNAREs Gs15, Syntaxin5 and Gos28, and Rab1b (GTPase involved in ER-Golgi and intra-Golgi transport [39]) showed minor partitioning and *cis*-Golgi SNAREs p27, Ers24 and rBet1 were not detected in the detergent-resistant fractions (Fig. 4A and B). When cells were extracted with Triton X-100, none of the proteins examined partitioned into caveolin-containing detergent-resistant fractions (Supplementary Fig. 2S).

Whereas most Golgi SNAREs are integral membrane proteins, Ykt6 is associated with the Golgi membranes via a dual farnesyl/palmitoyl lipid group [40]. Membrane binding of Ykt6 is under the negative intra-molecular regulation of its N-terminal domain that keeps the Ykt6 protein in cytosol [41]. To test whether Ykt6 is associated with detergent-resistant domains, we stably expressed GFP-(wild type Ykt6) and GFP-(F42EYkt6), the open conformation mutant [40], and subjected the cells to Lubrol WX solubilization. The wild type form of GFP-Ykt6 remained cytoplasmic and distributed to the detergent-soluble fraction, whereas GFP-(F42EYkt6) was membrane-bound and partitioned in detergent-resistant lipid fractions (Fig. 4C). We conclude that transmembrane Golgi SNARE proteins are primarily excluded from Lubrol-resistant lipid rafts.

2.3. Intra-Golgi mobility of SNARE proteins

Active retention through protein–protein or protein–lipid interactions may restrict SNARE mobility in the Golgi. To test intra-Golgi mobility of SNARE proteins, we photobleached small areas of the Golgi and followed the recovery of fluorescence as described [42] (Fig. 5A and Supplementary videos). Golgi SNAREs displayed differential mobility. The *cis*-Golgi *v*-SNARE rBet1 and the *trans*-Golgi *v*-SNARE Gs15 had the highest mobility and intra-Golgi *t*-SNAREs Syntaxin5 and Gos28 had the lowest mobility in the Golgi. The recovery of fluorescence after photobleaching Golgi regions for Syntaxin5 and Gos28 was very slow compared to other SNAREs (Fig. 5), suggesting that intra-Golgi SNAREs are largely immobile in the Golgi membranes. This result was reproduced in CHO cells (data not shown).

The *cis*-Golgi SNARE Ers24 was more mobile than the intra-Golgi SNARE Syntaxin5 and the *trans*-Golgi *v*-SNARE Gs15 was more mobile than the *trans*-Golgi *t*-SNAREs Syntaxin5 and Gos28 (Fig. 5B). This analysis suggests that *v*-SNAREs more mobile in the Golgi membranes than *t*-SNAREs.

Further analysis showed the linear relationship between intra-Golgi mobility rates and the rates of anterograde transport of SNARE proteins, consistent with the intra-Golgi distribution of SNAREs: Syntaxin5 < Gos28 < p27 < Ers24 < rBet1 (Fig. 5C). Similarly, intra-Golgi mobility rates correlated with the rates of retrograde transport of SNARE proteins (Fig. 5D). Thus, a selective Golgi retention mechanism may control intra-Golgi localization of SNARE proteins.

3. Discussion

3.1. SNARE recycling between the Golgi and the ER and fractional distillation hypothesis

The Golgi apparatus may utilize a fractional distillation principle for mediating protein sorting in the early secretory pathway [43]. This prediction leads to a new paradigm that the rate at which a Golgi protein enters the retrograde pathway and/or the rate at which an ER protein enters the Golgi may determine the relative partitioning of this protein into the *cis*- and *trans*-Golgi compartments. If this mechanism is true, then the *cis* < *trans* Golgi SNARE gradient is a result of a slower exit from and/or a faster return to the Golgi, while the *cis* > *trans* Golgi SNARE gradient is a result of a faster exit from and/or a slow return to the Golgi.

The present report, however, suggests that for all SNARE proteins examined, anterograde rates (K_{in}) were not significantly different than the corresponding retrograde rates (K_{out}) of transport (Fig. 1D, 3B and C). Thus, it is unlikely that the asymmetric

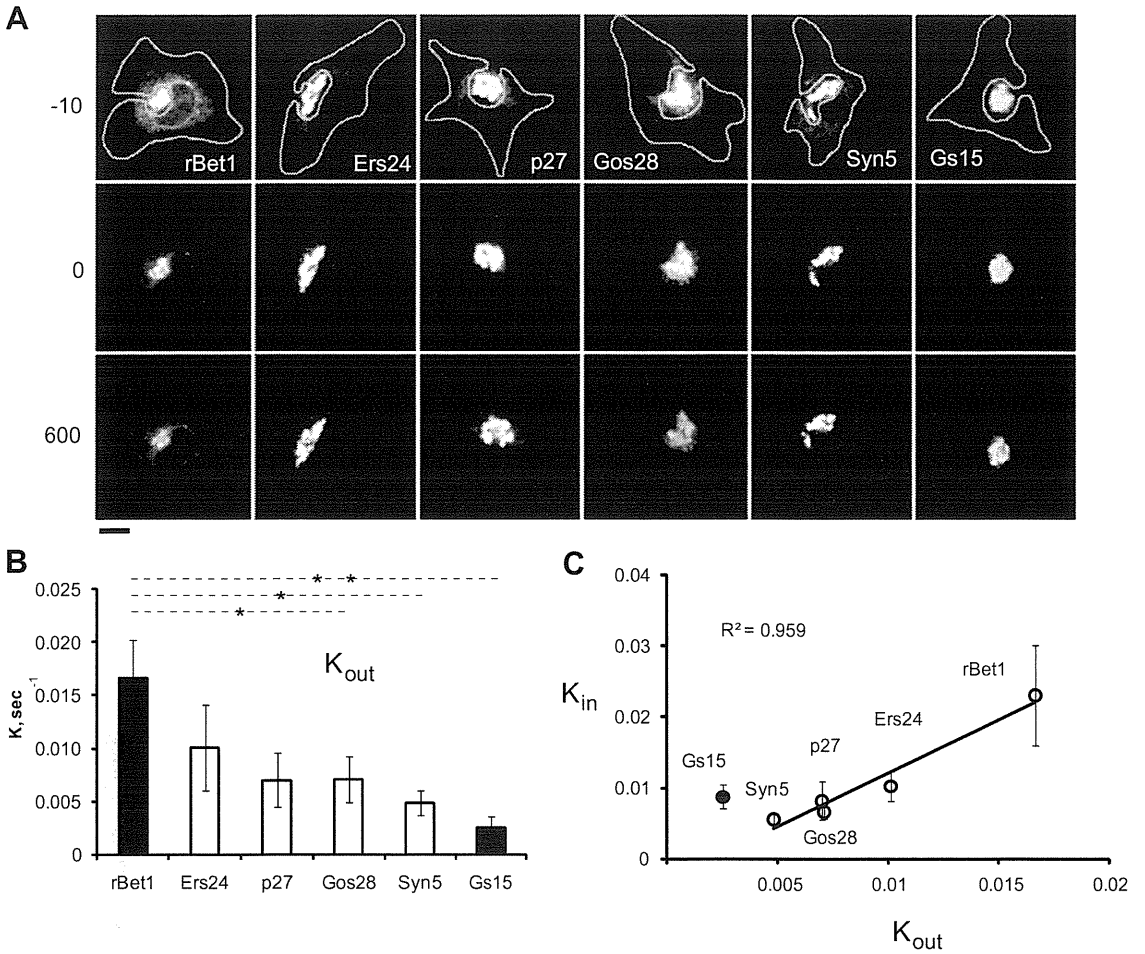

Fig. 3. Retrograde transport of SNARE proteins in the early secretory pathway. (A) CFP-tagged Golgi SNARE proteins were transiently expressed in NRK cells and retrograde transport rates were determined following the recovery of fluorescence in the ER after bleaching the ER (the regions of interest that exclude the Golgi). Representative images showing the pre-bleaching (−10 s), the post-bleaching (0 s), and the post-recovery stages (600 s) of FRAP. Scale bar = 10 μm. (B) The rates of retrograde transport of SNARE proteins. K_{out} values were calculated from single-exponential fits of fluorescence recovery curves after photobleaching the ER as described in Section 5. Bars are means ± S.E.M. for n = 10–15 cells. Statistically significant differences between K_{in} values were determined using One-way ANOVA; $^{*}P < 0.05$; $^{**}P < 0.01$. (C) Linear correlation between K_{in} (from Fig. 1D) and K_{out} (from Fig. 3B) for Golgi SNARE proteins.

anterograde–retrograde vesicular transport is involved in observed SNARE segregation in the early secretory pathway. Because the rates of anterograde and retrograde transport of SNARE proteins were similar, as expected for dynamic equilibrium, we hypothesize that SNAREs follow the constitutive recycling pathway between the Golgi and the ER. There was a linear relationship between intra-Golgi mobility rates and the rates of anterograde and retrograde transport of SNARE proteins, suggesting that the *cis*-Golgi SNAREs are more mobile in the Golgi than intra-Golgi SNAREs. Therefore we hypothesize that intra-Golgi retention controls SNARE release into the recycling pathway.

3.2. Partitioning of SNARE proteins in Golgi microdomains

It has been suggested that cholesterol concentration gradually increases from the *cis*-Golgi to the *trans*-Golgi [44]. The asymmetric distribution of cholesterol or other lipids alone the *cis–trans* axis of the Golgi may influence intra-Golgi mobility of SNARE proteins. The analysis of Lubrol-extracted cholesterol-containing lipid raft fractions revealed a high content of the endocytic pathway and TGN markers, including SNARE proteins Vti1 and Syntaxin 6, and non-SNARE proteins TGN38 and Rab6a (Fig. 4). In contrast, Golgi SNARE proteins showed poor partitioning or no partitioning into detergent-resistant fractions (Fig. 4). This finding was reproduced using two different cell lines. This result is consistent with a previous report that exocytic SNARE proteins Syntaxin 1 and Synaptobrevin 2 reconstituted into giant unilameller vesicles in vitro prefer the liquid-disordered phase [45]. Similar in vitro reconstitution experiments using purified Golgi SNAREs may unambiguously resolve the differences in membrane raft partitioning of *cis*-Golgi and *trans*-Golgi SNAREs in vitro.

Although protein partitioning into detergent-resistant membrane fractions is often used as the criterion for lipid raft association, this method is somewhat artificial in respect to the native state of biological membranes in vivo. While the TGN is enriched in lipid raft markers [46], the existence of intra-Golgi rafts, their composition, and the solubility in different detergents remain unknown. It is possible that differential mobility of Golgi SNARE proteins reflect the differences in membrane fluidity of individual Golgi cisternae rather than partitioning into lipid rafts. The length and amino acid composition of the transmembrane domains or differential homo and hetero oligomerization may guide SNARE proteins into different lipid domains of the Golgi membranes.

3.3. Intra-Golgi mobility of SNARE proteins and protein–protein interactions

It is now well documented that the intra-Golgi SNAREs interact genetically and physically with the Golgi tethering factors COG, GM130 and p115. These factors promote the assembly of SNARE

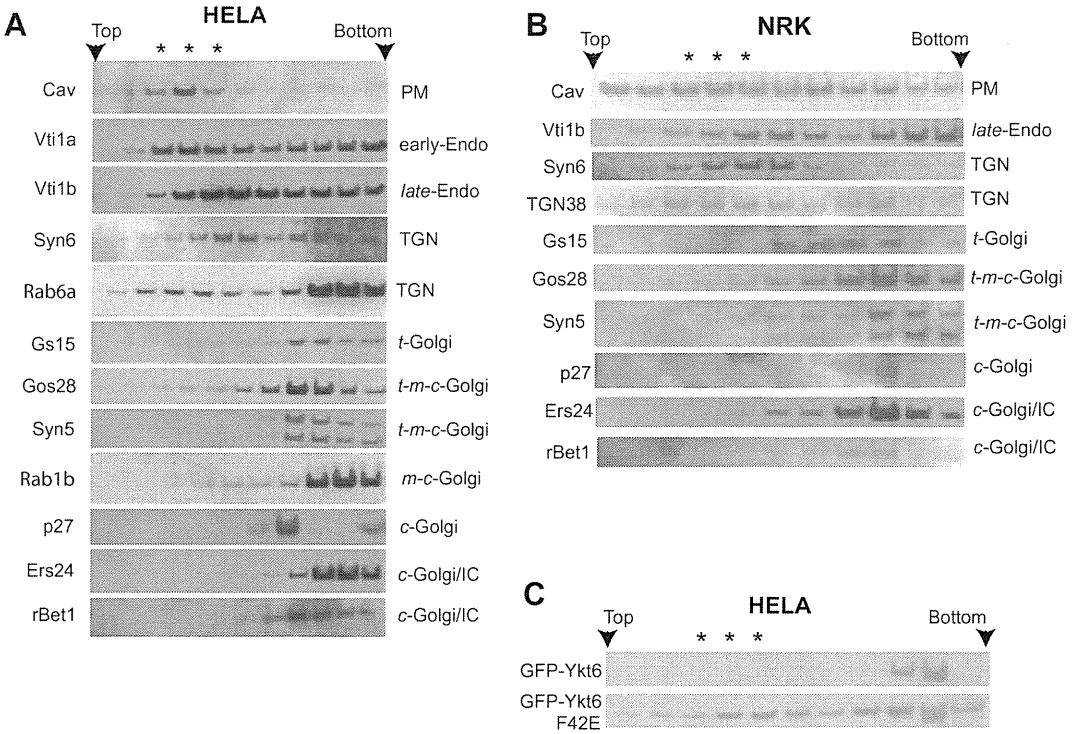

Fig. 4. SNARE partitioning in detergent-resistant membrane domains. Wild type HELA cells (A), HELA cells stably expressing GFP-Ykt6 or GFP-Ykt6-F42E (C), and wild type NRK cells (B) were lysed in the 1% Lubrol WX-containing buffer, and fractionated by sucrose density gradient ultracentrifugation as described in Section and Fig. 1S. Caveolin (Cav), Golgi SNAREs (Syntaxin5 (Syn5), p27, Ers24, rBet1, Gs15, and Gos28, GFP-tagged Ykt6s), TGN SNARE (Syntaxin6 (Syn6)), endosomal SNAREs (Vti1a and Vti1b), Rab1b, Rab6a and TGN38 levels in the resulting fractions were analyzed by immunoblot as described in Section 5. Asterisks indicate the position of Cav-containing detergent resistant rafts. PM, plasma membrane; early-Endo, early endosomes; late-Endo, late endosomes; TGN, *trans*-Golgi network; *t*-Golgi, *trans*-Golgi; *t-m-c*-Golgi, *trans, medial, cis*-Golgi compartments; IC, intermediate compartment.

complexes and localization of SNARE proteins to the Golgi (reviewed in [47]). Recent study suggests that Gos28 and Syntaxin5, but not Ers24, Bet1 and Gs15 bind the components of the COG complex in vivo [48]. This study agrees with the present report that Gos28 and Syntaxin5 have the lowest mobility, while rBet1, Ers24 and Gs15 have the highest mobility in the Golgi membranes (Fig. 5). We hypothesize that the *trans*-Golgi *t*-SNAREs *Gos28* and Syntaxin5 are stably associated with immobile fraction comprised of tethers and/or other Golgi proteins. In contrast, *v*-SNAREs rBet1 and Gs15 that don't bind the known tethers [48] have higher mobility in the Golgi (Fig. 5). The yeast homolog of the *trans*-Golgi *t*-SNAREs Ykt6 has been shown to bind the GOG complex in yeast [49], although its intra-Golgi mobility was not examined in the present study. Thus, the spatial segregation of the *cis*-Golgi and *trans*-Golgi SNAREpins correlate with their differential association with the Golgi tethering factors.

Homo and hetero oligomerization of SNARE proteins via their transmembrane or cytoplasmic domains may also contribute to their localization mechanism in the Golgi. Although numerous co-immunoprecipitation studies suggest that *trans*-SNARE complexes are relatively unabundant in the cell, one can argue that detergent solubilization may disrupt weak protein–protein interactions that bind SNARE proteins in a delicate protein network, consisting of fusogenic and inhibitory SNARE partners and Golgi tethers. These weak, possibly transient interactions may hold SNARE proteins in place and also regulate fusion specificity of membrane compartments.

3.4. Golgi localization of SNARE proteins and i-SNARE hypothesis

Although vesicle recycling and/or association with Golgi proteins or lipids may modulate the steady-state levels of SNARE proteins in the Golgi, one additional mechanism remains untested in vivo. We previously described a new functional class of SNAREs, designated inhibitory SNAREs (*i*-SNAREs) [27]. An *i*-SNARE inhibits membrane fusion by substituting for a subunit of a fusogenic SNARE complex to form a non-fusogenic complex. For example, the *cis*-Golgi SNAREs Bet1 and p27 function as the *i*-SNAREs that inhibit fusion mediated by the *trans*-Golgi SNAREs, and the *trans*-Golgi SNAREs Gs15 and Gos28 function as the *i*-SNAREs that inhibit fusion mediated by the *cis*-Golgi SNAREs [27].

This finding has two strong implications that (i) SNAREs can mediate topologically restricted membrane fusion, and (ii) SNAREs can regulate their own distribution in the Golgi stack. *i*-SNAREs may also drive the homotypic fusion of *trans*-Golgi membranes by restricting fusion of vesicles enriched in the *cis*-Golgi SNAREs with the *trans*-Golgi compartments, and by allowing fusion of vesicles enriched in the *trans*-Golgi SNAREs with the *trans*-Golgi compartments. The same rule may apply to the homotypic fusion in the *cis*-Golgi. This process may lead to formation of non-identical compartments and the apparent gradient-like distribution of SNARE proteins across the Golgi stack. Because the yeast Golgi is not assembled in a pancake-like structure of the mammalian Golgi, it is possible that homotypic assembly of Golgi compartments, in the absence of their spatial alignment, is sufficient for mediating Golgi function, including cargo sorting and protein glycosylation. The question arises as whether the inhibitor–activator relationship exists among the other classes of Golgi proteins and how the homotypic and heterotypic ensembles of SNARE proteins regulate self-organization of the Golgi.

3.5. SNARE sorting into different transport vesicles

The mechanisms, which explain the different transport rates of SNARE proteins, remain unclear. It is possible that vesicle fusion specificity (reflected by different transport rates) can be

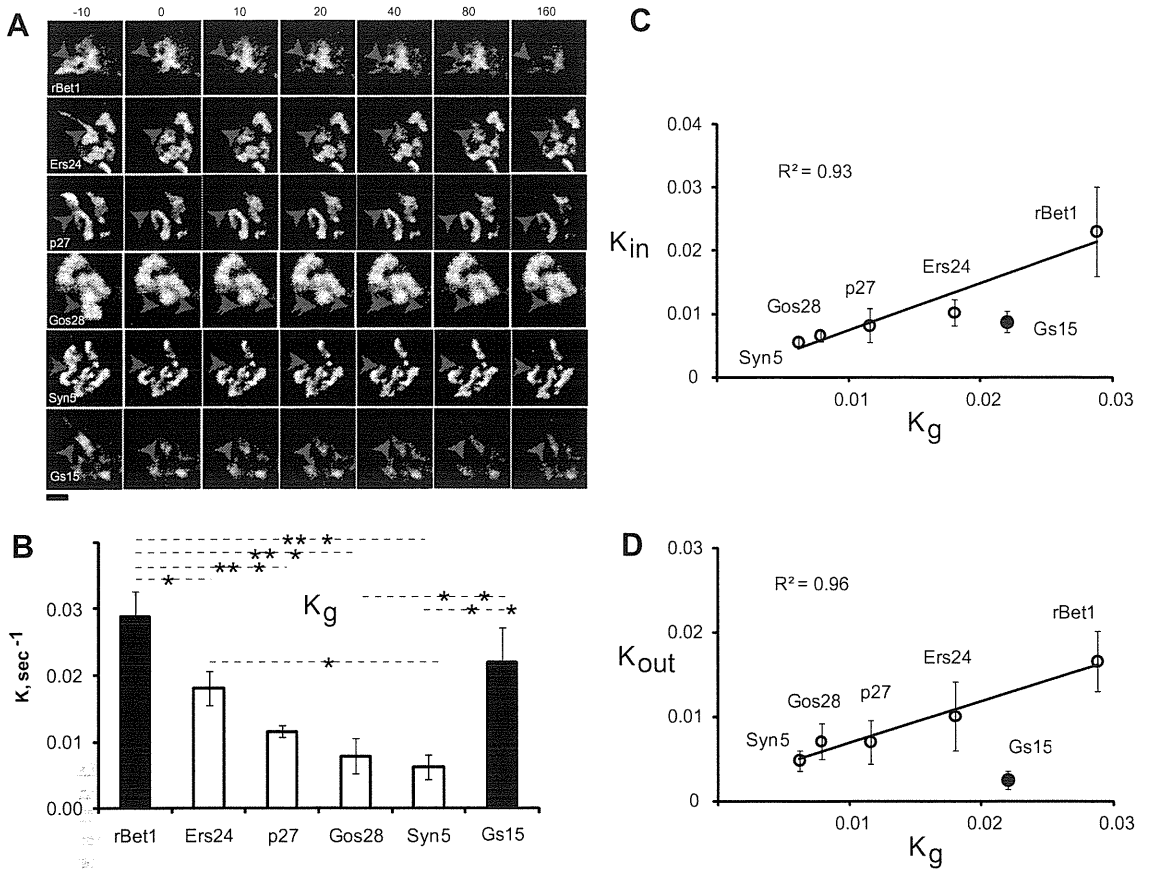

Fig. 5. Intra-Golgi mobility of SNARE proteins. (A) CFP-tagged Golgi SNARE proteins were transiently expressed in NRK cells and intra-Golgi transport rates were determined following fluorescence recovery of small photobleached Golgi regions (marked with arrowheads) as described in Section 5. The time course of fluorescence recovery is shown in seconds. B) K_g values were calculated from single-exponential fits of fluorescence recovery curves after photobleaching parts of the Golgi. Bars are means ± S.E.M. for $n = 10–15$. Statistically significant differences between K_{in} values were determined using One-way ANOVA; $^{*}P < 0.05$; $^{**}P < 0.01$; $^{***}P < 0.001$. (C) Linear correlation between K_{in} (from Fig. 1D) and K_g (from Fig. 5B) for Golgi SNARE proteins. (D) Linear correlation between K_{out} (from Fig. 3B) and K_g (from Fig. 5B) for Golgi SNARE proteins. The rates = s^{-1}.

programmed during SNARE sorting into different types of transport vesicles in the Golgi. For instance, rBet1 and GS15 may bind the *cis*-Golgi and *trans*-Golgi sets of coat proteins, respectively, guiding *cis*-Golgi and *trans*-Golgi v-SNAREs into different populations of Golgi-derived COPI vesicles [50–52]. Intra-Golgi SNAREs might enter both the *cis*-Golgi and the *trans*-Golgi types of COPI vesicles, although the third "mixed" type of COPI vesicles involved in intra-Golgi sorting of SNAREs may also exist.

A similar type of the sorting mechanism operating at the vesicle budding sites in the ER may drive the *cis*-Golgi *v*-SNARE rBet1 into a distinct (and possibly more fusogenic) type of COPII vesicles, resulting in the segregation of rBet1 from other SNAREs [53,54], explaining faster recovery rates for rBet1 in the Golgi. It is noteworthy that the *i*-SNARE-mediated mechanism might preclude undesirable fusion events between different types of vesicles by keeping a subset of SNAREs in a passive "passenger" mode.

4. Conclusions

Unfortunately, the FRAP-based method alone cannot resolve the mechanism of intra-Golgi transport of SNARE proteins. The measured transport rates in the Golgi might reflect the number of transport steps within the Golgi which may occur by several independent mechanisms, including vesicle- or tubule-mediated transport, lateral diffusion in the Golgi membranes, or cisternae maturation (reviewed in [55,56]). It is likely that a combination of these mechanisms contribute to SNARE localization. Other methods that involve super-resolution imaging and reversible inactivation of the Golgi proteins are required to unambiguously resolve the mechanisms of intra-Golgi transport of SNARE proteins [57].

5. Materials and methods

5.1. Recombinant techniques, cell culture and protein expression

The coding regions of rat Bet1, p27, and Syntaxin5, mouse Gs15, Chinese hamster Gos28 and Ers24 have been subcloned in frame into BamH1/Mlu1 sites of modified (Mlu1 site was introduced between BamH1 and Xba1) pECFP-C1 or SacII/BamH1 sites of pECFP-N1 vectors (Clontech Laboratories Inc., Mountain View USA). Similar GFP-SNARE constructs have been described [29]. NRK cells were cultured in 8-well chambers (Lab-Tek II chambered #1.5, German coverglass system, Nalge Nunc International, Rochester, NY, USA) in DMEM containing 10% fetal calf serum, penicillin, streptomycin, and fungizone (Invitrogen, Grand Island, NY, USA). Cells were transfected with 2 μg DNA using FuGENE HD transfection reagent (Promega Corporation, Madison, USA) and assayed within 24 h after transfection. Only cells expressing low levels of CFP-tagged proteins were used for analysis.

5.2. Live-cell microscopy and image analysis

Image recording was conducted using an inverted Leica SP5 AOBS spectral confocal system equipped with a motorized, temperature-controlled stage and 63x HCX PL APO (NE = 1.451)

glycerol objectives. CFP was excited with an Argon laser, and images were recorded at emission bandwidth of 500–550 nm. Photobleaching was performed using the built-in FRAP module of the Leica confocal microscope. Anterograde (K_{in}), retrograde (K_{out}), and intra-Golgi (K_g) rates of transport were calculated as follows. Raw fluorescent values obtained from the post-bleach recovery traces (F_{pb}) were background (F_b)-corrected and initial fluorescence values (F_0) were set to zero:

$$F = (F_{pb} - F_b) - (F_0 - F_b)$$

The corrected traces were used for rate (K) calculations using the single exponential fit function in GraphPad Prism, version-4 software:

$$F = F_{max}(1 - e^{-Kt})$$

The goodness of fit was determined using the R^2 values. Cells that displayed focus shift or movements during the recovery of fluorescence were not included in analysis.

5.3. Flotation of lipid raft fractions

Lipid raft fractions were separated as described previously [58] with 1% (v/v) Lubrol WX instead of Triton X-100 as a detergent. In brief, sub-confluent HeLa cells in two 10 cm-dishes, after being washed with PBS, were harvested by scraping and precipitated by centrifugation at 300×*g* for 5 min. The precipitated cells were extracted with 100 μl of 1% (v/v) Lubrol WX in MN buffer (25 mM MES-NaOH, pH 6.5) containing 0.15 M NaCl and a protease inhibitor cocktail (Complete™ EDTA-free, Roche) for 30 min on ice. Cell extracts were diluted into 500 μl, by adding 85% (w/v) sucrose in MN buffer, and layered under 8 ml of a 10–30% sucrose gradient in MN buffer. After centrifugation at 75000×*g* for 20 h at 4 °C, 0.75-ml fractions were collected from the top of the resulting gradient.

5.4. Antibodies

Rabbit polyclonal antibody against Caveolin was purchased from Santa Cruz Biotechnology. Mouse monoclonal antibodies against Vti1a and Vti1b were from BD Biosciences, against rBet1 (clone 16G6) from StressGen Biotechnology, and against GFP from Roche Applied Science. Mouse monoclonal antibodies against Rab1b (clone M1E7) and Rab6a (clone 5B10) were gifted from T. Mayer [59]. Rabbit polyclonal antibodies against Gos28, Syntaxin5, Ers24, p27, Syntaxin 6, and Gs15 were generated and affinity-purified as described previously [60].

5.5. Immunoblot analysis

Each fraction was solubilized with NuPAGE LDS sample buffer (Invitrogen) containing 50 mM DTT and then heated at 95 °C for 5 min. Electrophoresis of these samples was performed in precast NuPAGE 10% or 12% bis–tris gels (Invitrogen). For immunoblot analysis, the proteins were transferred to polyvinylidene difluoride membranes (Invitrogen), and the blotted membrane was incubated with primary antibodies, at a 1:1000 dilution, for 90 min. Horseradish peroxidase-conjugated secondary antibody (GE healthcare), at a 1:1000 dilution, was incubated with the blot for 90 min. Detection was performed by using ECL (GE Healthcare) and fluorography.

5.6. Cell culture and establishment of GFP-tagged Ykt6-expressing cells

All cells were grown in Dulbecco's modified Eagle's medium (DMEM) supplemented with 10% fetal bovine serum (FBS), 100 U/ml Penicillin G, and 100 mg/ml streptomycin sulfate under a 5% CO_2 atmosphere at 37 °C. Mammalian expression vectors of GFP-tagged Ykt6 and Ykt6-F42E were constructed as described previously [40]. To establish cells stably expressing GFP-Ykt6 or GFP-Ykt6-F42E, HeLa cells were transfected with these plasmids using FuGENE 6 Transfection Reagent (Roche), selected by G418 resistance, and cloned. Exogenous Ykt6 expression in these cell clones was confirmed by fluorescent microscopy.

5.7. Permeabilized cell assay

NRK cells were permeabilized as described [61]. Briefly, cells were rinsed with cold KHM buffer (25 mM HEPES pH 7.4, 125 mM potassium acetate, 2.5 mM magnesium acetate), and incubated for 10 min on ice in the presence of 30 μg/ml digitonin (Calbiochem) in KHM buffer. In NSF rescue experiments, 0.2 mM NEM was added to a permeabilazation mixture. NEM was neutralized by 0.4 mM DTT for 5 min. Cells were rinsed with cold KHM buffer, and then incubated for 10–20 min on ice in 200 μl transport mixture (5 mM ATP, ATP-regenerating system, 50% bovine brain cytosol, KHM buffer, 5–10 μg NSF and 5–10 μg alpha-SNAP). Recombinant Sar1 mutant (Sar1 T39N) was purified as described [62] and dialyzed against KHM buffer containing 10 μM GDP and 0.5 mM DTT. Ten to twenty micrograms of Sar1 T39N was added to a transport mixture.

Appendix A. Supplementary data

Supplementary data associated with this article can be found, in the online version, at http://dx.doi.org/10.1016/j.febslet.2013.06.004.

References

[1] Rothman, J.E. and Wieland, F.T. (1996) Protein sorting by transport vesicles. Science 272, 227–234.
[2] Lippincott-Schwartz, J., Yuan, L.C., Bonifacino, J.S. and Klausner, R.D. (1989) Rapid redistribution of Golgi proteins into the ER in cells treated with brefeldin A: evidence for membrane cycling from Golgi to ER. Cell 56, 801–813.
[3] Dean, N. and Pelham, H.R. (1990) Recycling of proteins from the Golgi compartment to the ER in yeast. J. Cell Biol. 111, 369–377.
[4] Lewis, M.J. and Pelham, H.R. (1992) Ligand-induced redistribution of a human KDEL receptor from the Golgi complex to the endoplasmic reticulum. Cell 68, 353–364.
[5] Hammond, C. and Helenius, A. (1994) Quality control in the secretory pathway: retention of a misfolded viral membrane glycoprotein involves cycling between the ER, intermediate compartment, and Golgi apparatus. J. Cell Biol. 126, 41–52.
[6] Scales, S.J., Pepperkok, R. and Kreis, T.E. (1997) Visualization of ER-to-Golgi transport in living cells reveals a sequential mode of action for COPII and COPI. Cell 90, 1137–1148.
[7] Cole, N.B., Ellenberg, J., Song, J., DiEuliis, D. and Lippincott-Schwartz, J. (1998) Retrograde transport of Golgi-localized proteins to the ER. J. Cell Biol. 140, 1–15.
[8] Storrie, B., White, J., Rottger, S., Stelzer, E.H., Suganuma, T. and Nilsson, T. (1998) Recycling of golgi-resident glycosyltransferases through the ER reveals a novel pathway and provides an explanation for nocodazole-induced Golgi scattering. J. Cell Biol. 143, 1505–1521.
[9] Todorow, Z., Spang, A., Carmack, E., Yates, J. and Schekman, R. (2000) Active recycling of yeast Golgi mannosyltransferase complexes through the endoplasmic reticulum. Proc. Natl. Acad. Sci. USA 97, 13643–13648.
[10] Sollner, T., Whiteheart, S.W., Brunner, M., Erdjument-Bromage, H., Geromanos, S., Tempst, P. and Rothman, J.E. (1993) SNAP receptors implicated in vesicle targeting and fusion. Nature 362, 318–324.
[11] Newman, A.P. and Ferro-Novick, S. (1987) Characterization of new mutants in the early part of the yeast secretory pathway isolated by a [3H]mannose suicide selection. J. Cell Biol. 105, 1587–1594.
[12] Hay, J.C., Hirling, H. and Scheller, R.H. (1996) Mammalian vesicle trafficking proteins of the endoplasmic reticulum and Golgi apparatus. J. Biol. Chem. 271, 5671–5679.
[13] Kaiser, C.A. and Schekman, R. (1990) Distinct sets of SEC genes govern transport vesicle formation and fusion early in the secretory pathway. Cell 61, 723–733.

[14] Lowe, S.L., Peter, F., Subramaniam, V.N., Wong, S.H. and Hong, W. (1997) A SNARE involved in protein transport through the Golgi apparatus. Nature 389, 881–884.
[15] Hay, J.C., Chao, D.S., Kuo, C.S. and Scheller, R.H. (1997) Protein interactions regulating vesicle transport between the endoplasmic reticulum and Golgi apparatus in mammalian cells. Cell 89, 149–158.
[16] Bennett, M.K., Calakos, N. and Scheller, R.H. (1992) Syntaxin: a synaptic protein implicated in docking of synaptic vesicles at presynaptic active zones. Science 257, 255–259.
[17] Hardwick, K.G. and Pelham, H.R. (1992) SED5 encodes a 39-kD integral membrane protein required for vesicular transport between the ER and the Golgi complex. J. Cell Biol. 119, 513–521.
[18] Nagahama, M., Orci, L., Ravazzola, M., Amherdt, M., Lacomis, L., Tempst, P., Rothman, J.E. and Sollner, T.H. (1996) A *v*-SNARE implicated in intra-Golgi transport. J. Cell Biol. 133, 507–516.
[19] Subramaniam, V.N., Peter, F., Philp, R., Wong, S.H. and Hong, W. (1996) GS28, a 28-kilodalton Golgi SNARE that participates in ER-Golgi transport. Science 272, 1161–1163.
[20] McNew, J.A., Coe, J.G., Sogaard, M., Zemelman, B.V., Wimmer, C., Hong, W. and Sollner, T.H. (1998) Gos1p, a *Saccharomyces cerevisiae* SNARE protein involved in Golgi transport. FEBS Lett. 435, 89–95.
[21] McNew, J.A. et al. (1997) Ykt6p, a prenylated SNARE essential for endoplasmic reticulum–Golgi transport. J. Biol. Chem. 272, 17776–17783.
[22] Banfield, D.K., Lewis, M.J. and Pelham, H.R. (1995) A SNARE-like protein required for traffic through the Golgi complex. Nature 375, 806–809.
[23] Subramaniam, V.N., Loh, E. and Hong, W. (1997) *N*-Ethylmaleimide-sensitive factor (NSF) and alpha-soluble NSF attachment proteins (SNAP) mediate dissociation of GS28-syntaxin 5 Golgi SNAP receptors (SNARE) complex. J. Biol. Chem. 272, 25441–25444.
[24] Parlati, F., McNew, J.A., Fukuda, R., Miller, R., Sollner, T.H. and Rothman, J.E. (2000) Topological restriction of SNARE-dependent membrane fusion. Nature 407, 194–198.
[25] Zhang, T. and Hong, W. (2001) Ykt6 forms a SNARE complex with Syntaxin 5, GS28, and Bet1 and participates in a late stage in endoplasmic reticulum–Golgi transport. J. Biol. Chem. 276, 27480–27487.
[26] Parlati, F., Varlamov, O., Paz, K., McNew, J.A., Hurtado, D., Sollner, T.H. and Rothman, J.E. (2002) Distinct SNARE complexes mediating membrane fusion in Golgi transport based on combinatorial specificity. Proc. Natl. Acad. Sci. USA 99, 5424–5429.
[27] Varlamov, O. et al. (2004) I-SNAREs: inhibitory SNAREs that fine-tune the specificity of membrane fusion. J. Cell Biol. 164, 79–88.
[28] Lippincott-Schwartz, J., Altan-Bonnet, N. and Patterson, G.H. (2003) Photobleaching and photoactivation: following protein dynamics in living cells. Nat. Cell Biol. (Suppl. S7–S14).
[29] Chao, D.S., Hay, J.C., Winnick, S., Prekeris, R., Klumperman, J. and Scheller, R.H. (1999) SNARE membrane trafficking dynamics in vivo. J. Cell Biol. 144, 869–881.
[30] Barlowe, C. and Schekman, R. (1993) SEC12 encodes a guanine-nucleotide-exchange factor essential for transport vesicle budding from the ER. Nature 365, 347–349.
[31] Kuge, O. et al. (1994) Sar1 promotes vesicle budding from the endoplasmic reticulum but not Golgi compartments. J. Cell Biol. 125, 51–65.
[32] Lafont, F., Verkade, P., Galli, T., Wimmer, C., Louvard, D. and Simons, K. (1999) Raft association of SNAP receptors acting in apical trafficking in Madin–Darby canine kidney cells. Proc. Natl. Acad. Sci. USA 96, 3734–3738.
[33] Lang, T., Bruns, D., Wenzel, D., Riedel, D., Holroyd, P., Thiele, C. and Jahn, R. (2001) SNAREs are concentrated in cholesterol-dependent clusters that define docking and fusion sites for exocytosis. EMBO J. 20, 2202–2213.
[34] Chamberlain, L.H., Burgoyne, R.D. and Gould, G.W. (2001) SNARE proteins are highly enriched in lipid rafts in PC12 cells: implications for the spatial control of exocytosis. Proc. Natl. Acad. Sci. USA 98, 5619–5624.
[35] Puri, N. and Roche, P.A. (2006) Ternary SNARE complexes are enriched in lipid rafts during mast cell exocytosis. Traffic 7, 1482–1494.
[36] Murray, D.H. and Tamm, L.K. (2009) Clustering of syntaxin-1A in model membranes is modulated by phosphatidylinositol 4,5-bisphosphate and cholesterol. Biochemistry 48, 4617–4625.
[37] Williams, T.M. and Lisanti, M.P. (2004) The caveolin proteins. Genome Biol. 5, 214.
[38] Jahn, R. and Scheller, R.H. (2006) SNAREs – engines for membrane fusion. Nat. Rev. Mol. Cell Biol. 7, 631–643.
[39] Mizuno-Yamasaki, E., Rivera-Molina, F. and Novick, P. (2012) GTPase Networks in Membrane Traffic. Annu. Rev. Biochem..
[40] Fukasawa, M., Varlamov, O., Eng, W.S., Sollner, T.H. and Rothman, J.E. (2004) Localization and activity of the SNARE Ykt6 determined by its regulatory domain and palmitoylation. Proc. Natl. Acad. Sci. USA 101, 4815–4820.
[41] Wen, W. et al. (2010) Lipid-induced conformational switch controls fusion activity of longin domain SNARE Ykt6. Mol. Cell 37, 383–395.
[42] Cole, N.B., Smith, C.L., Sciaky, N., Terasaki, M., Edidin, M. and Lippincott-Schwartz, J. (1996) Diffusional mobility of Golgi proteins in membranes of living cells. Science 273, 797–801.
[43] Rothman, J.E. (1981) The Golgi apparatus: two organelles in tandem. Science 213, 1212–1219.
[44] Mesmin, B. and Maxfield, F.R. (2009) Intracellular sterol dynamics. Biochim. Biophys. Acta 1791, 636–645.
[45] Bacia, K., Schuette, C.G., Kahya, N., Jahn, R. and Schwille, P. (2004) SNAREs prefer liquid-disordered over "raft" (liquid-ordered) domains when reconstituted into giant unilamellar vesicles. J. Biol. Chem. 279, 37951–37955.
[46] Simons, K. and Gerl, M.J. (2010) Revitalizing membrane rafts: new tools and insights. Nat. Rev. Mol. Cell Biol. 11, 688–699.
[47] Sztul, E. and Lupashin, V. (2009) Role of vesicle tethering factors in the ER–Golgi membrane traffic. FEBS Lett. 583, 3770–3783.
[48] Willett, R., Kudlyk, T., Pokrovskaya, I., Schonherr, R., Ungar, D., Duden, R. and Lupashin, V. (2013) COG complexes form spatial landmarks for distinct SNARE complexes. Nat. Commun. 4, 1553.
[49] Suvorova, E.S., Duden, R. and Lupashin, V.V. (2002) The Sec34/Sec35p complex, a Ypt1p effector required for retrograde intra-Golgi trafficking, interacts with Golgi SNAREs and COPI vesicle coat proteins. J. Cell Biol. 157, 631–643.
[50] Moelleken, J. et al. (2007) Differential localization of coatomer complex isoforms within the Golgi apparatus. Proc. Natl. Acad. Sci. USA 104, 4425–4430.
[51] Rutz, C., Satoh, A., Ronchi, P., Brugger, B., Warren, G. and Wieland, F.T. (2009) Following the fate in vivo of COPI vesicles generated in vitro. Traffic 10, 994–1005.
[52] Beck, R., Rawet, M., Wieland, F.T. and Cassel, D. (2009) The COPI system: molecular mechanisms and function. FEBS Lett. 583, 2701–2709.
[53] Mossessova, E., Bickford, L.C. and Goldberg, J. (2003) SNARE selectivity of the COPII coat. Cell 114, 483–495.
[54] Mancias, J.D. and Goldberg, J. (2007) The transport signal on Sec22 for packaging into COPII-coated vesicles is a conformational epitope. Mol. Cell 26, 403–414.
[55] Glick, B.S. and Nakano, A. (2009) Membrane traffic within the Golgi apparatus. Annu. Rev. Cell Dev. Biol. 25, 113–132.
[56] Banfield, D.K. (2011) Mechanisms of protein retention in the Golgi. Cold Spring Harb. Perspect. Biol. 3, a005264.
[57] Rothman, J.E. (2010) The future of Golgi research. Mol. Biol. Cell 21, 3776–3780.
[58] Fukasawa, M., Nishijima, M., Itabe, H., Takano, T. and Hanada, K. (2000) Reduction of sphingomyelin level without accumulation of ceramide in Chinese hamster ovary cells affects detergent-resistant membrane domains and enhances cellular cholesterol efflux to methyl-beta – cyclodextrin. J. Biol. Chem. 275, 34028–34034.
[59] Elazar, Z., Mayer, T. and Rothman, J.E. (1994) Removal of Rab GTP-binding proteins from Golgi membranes by GDP dissociation inhibitor inhibits intercisternal transport in the Golgi stacks. J. Biol. Chem. 269, 794–797.
[60] Volchuk, A. et al. (2004) Countercurrent distribution of two distinct SNARE complexes mediating transport within the Golgi stack. Mol. Biol. Cell 15, 1506–1518.
[61] Acharya, U., Mallabiabarrena, A., Acharya, J.K. and Malhotra, V. (1998) Signaling via mitogen-activated protein kinase kinase (MEK1) is required for Golgi fragmentation during mitosis. Cell 92, 183–192.
[62] Rowe, T. and Balch, W.E. (1995) Expression and purification of mammalian Sarl. Methods Enzymol. 257, 49–53.

European Journal of Pharmacology 724 (2014) 161–167

Contents lists available at ScienceDirect

European Journal of Pharmacology

journal homepage: www.elsevier.com/locate/ejphar

Pulmonary, gastrointestinal and urogenital pharmacology

Ursodeoxycholic acid inhibits overexpression of P-glycoprotein induced by doxorubicin in HepG2 cells

Yuki Komori [a], Sakiko Arisawa [a], Miho Takai [a], Kunihiro Yokoyama [a], Minako Honda [a], Kazuhiko Hayashi [b], Masatoshi Ishigami [b], Yoshiaki Katano [b], Hidemi Goto [b], Jun Ueyama [a], Tetsuya Ishikawa [a], Shinya Wakusawa [a,*]

[a] Division of Medical Laboratory Sciences, Department of Radiological and Medical Laboratory Sciences, Nagoya University Graduate School of Medicine, 1-1-20 Daiko-minami, Higashi-ku, Nagoya 461-8673, Japan
[b] Division of Gastroenterology, Department of Internal Medicine, Nagoya University Graduate School of Medicine, 65 Tsurumai-cho, Showa-ku, Nagoya 466-8550, Japan

ARTICLE INFO

Article history:
Received 8 October 2013
Received in revised form
12 December 2013
Accepted 12 December 2013
Available online 24 December 2013

Chemical compounds studied in this article:
Ursodeoxycholic acid (PubChem CID: 31401)
Chenodeoxycholic acid (PubChem CID: 10133)
Deoxycholic acid (PubChem CID: 222528)
Lithocholic acid (PubChem CID: 9903)
Doxorubicin (PubChem CID: 31703)
Rhodamine 123 (PubChem CID: 65217)

Keywords:
Bile acids
P-Glycoprotein
Reactive oxygen species
MDR1
Ursodeoxycholic acid

ABSTRACT

The hepatoprotective action of ursodeoxycholic acid (UDCA) was previously suggested to be partially dependent on its antioxidative effect. Doxorubicin (DOX) and reactive oxygen species have also been implicated in the overexpression of P-glycoprotein (P-gp), which is encoded by the MDR1 gene and causes antitumor multidrug resistance. In the present study, we assessed the effects of UDCA on the expression of MDR1 mRNA, P-gp, and intracellular reactive oxygen species levels in DOX-treated HepG2 cells and compared them to those of other bile acids. DOX-induced increases in reactive oxygen species levels and the expression of MDR1 mRNA were inhibited by N-acetylcysteine, an antioxidant, and the DOX-induced increase in reactive oxygen species levels and DOX-induced overexpression of MDR1 mRNA and P-gp were inhibited by UDCA. Cells treated with UDCA showed improved rhodamine 123 uptake, which was decreased in cells treated with DOX alone. Moreover, cells exposed to DOX for 24 h combined with UDCA accumulated more DOX than that of cells treated with DOX alone. Thus, UDCA may have inhibited the overexpression of P-gp by suppressing DOX-induced reactive oxygen species production. Chenodeoxycholic acid (CDCA) also exhibited these effects, whereas deoxycholic acid and litocholic acid were ineffective. In conclusion, UDCA and CDCA had an inhibitory effect on the induction of P-gp expression and reactive oxygen species by DOX in HepG2 cells. The administration of UDCA may be beneficial due to its ability to prevent the overexpression of reactive oxygen species and acquisition of multidrug resistance in hepatocellular carcinoma cells.

1. Introduction

Ursodeoxycholic acid (UDCA) is a tertiary bile acid in humans, and large doses have been used as a hepatoprotective drug in the treatment of antivirus therapy non-responsive chronic hepatitis C (Omata et al., 2007) and primary biliary cirrhosis (Corpechot et al., 2000). Although the detailed mechanism of its hepatoprotective effect remains to be clarified, it may be due to its antioxidative effect and protection against apoptosis caused by mitochondria injury (Mitsuyoshi et al., 1999; Rajesh et al., 2005; Okada et al., 2008; Kawata et al., 2010). As a molecular mechanism for its antioxidative effect, we recently demonstrated that UDCA induced glutathione (GSH) synthesis due to the translocation of Nrf2 into the nucleus following activation of the PI3K/Akt pathway (Arisawa et al., 2009), which may also contribute to the protection of mitochondria.

P-Glycoprotein (P-gp), a membrane drug transporter encoded by the MDR1 gene, is frequently overexpressed in tumor cells treated with chemotherapeutic agents including anthracyclines such as doxorubicin (DOX) and causes antitumor multidrug resistance (Hu et al., 1995). The physiological expression of P-gp has also been reported in various epithelial cells and it has been shown to play a role in the regulation of absorption or excretion of small amphipathic chemical compounds in organs such as the kidneys and liver (Borst and Elferink, 2002). Overexpression of the MDR1 gene was previously shown to be induced by reactive oxygen species in primary cultures of rat hepatocytes (Ziemann et al., 1999), while DOX is known to increase intracellular reactive oxygen species levels in several cells (Myers et al., 1977; Bates and

* Corresponding author. Tel./fax: +81 52 719 1558.
E-mail address: wakusawa@met.nagoya-u.ac.jp (S. Wakusawa).

0014-2999/$ - see front matter © 2013 Elsevier B.V. All rights reserved.
http://dx.doi.org/10.1016/j.ejphar.2013.12.023

Winterbourn, 1982; Ortiz et al., 2008) and decrease GSH levels in rat hepatoma cells (Ortiz et al., 2008). Hepatocellular carcinoma is the third leading cause of cancer-related death in the world (Jemal et al., 2011). Hepatitis C is a major risk factor for hepatocellular carcinoma, and DOX is frequently used as a chemotherapeutic agent in the case of transarterial chemoembolism for this disease (Tinkle and Haas-Kogan, 2012).

DOX was previously suggested to induce reactive oxygen species and P-gp; therefore, reactive oxygen species has been associated with the induction of P-gp in DOX-treated cells. In addition, because UDCA exhibits antioxidative effects, it may down-regulate the overexpression of P-gp and suppress the induction of multidrug resistance by DOX. However, the effect of UDCA on the expression or/and function of P-gp in DOX-treated hepatoma cells has not yet been examined. In this study, to evaluate the efficacy of UDCA on DOX-induced elevations in P-gp and reactive oxygen species levels, we firstly examined the effect of N-acetylcysteine (NAC), an antioxidant, on DOX-induced elevations in P-gp levels and then investigated the effects of UDCA on human hepatoma HepG2 cells. In addition, we also investigated the effects of chenodeoxycholic acid (CDCA), deoxycholic acid (DCA), and litocholic acid (LCA) to compare the effects of UDCA with those of other bile acids.

2. Materials and methods

2.1. Chemicals

UDCA was kindly supplied by Tanabe-Mitsubishi Pharmaceuticals (Osaka, Japan). CDCA, DCA, LCA, DOX, 6-carboxy-2′, 7′-1 dichlorodihydrofluorescein (CDCFH), NAC, and rhodamine 123 (Rho123) were purchased from Sigma Japan (Tokyo, Japan).

2.2. Cell culture

Human hepatoma HepG2 cells were cultured in Dulbecco's modified Eagle's medium (Sigma, Japan) supplemented with 5% (v/v) heat-inactivated fetal calf serum (BioWest, Nauille, France), 100 U/ml of penicillin (Invitrogen Japan, Tokyo, Japan), 100 μg/ml of streptomycin (Invitrogen Japan), and 0.25 mg/ml of amphotericin B (Invitrogen Japan) in 35-mm plastic dishes in the presence of 5% CO_2 at 37 °C until semi-confluency. Varying concentrations of agents were then added to the culture medium, and cells were cultured for the designated periods. Bile acids were initially dissolved in dimethylsulfoxide (DMSO, Sigma Japan) at an appropriate concentration and were then added to the culture medium. The concentration of DMSO was adjusted to 0.1% (v/v) of the culture medium in each group.

2.3. Determination of intracellular reactive oxygen species

Reactive oxygen species levels were quantified in cells using CDCFH (10 μM) as described previously (Arisawa et al., 2009). The fluorescence of CDCF was measured at 480 nm/538 nm (emission/excitation). The results were obtained as the content (nmol) per mg protein and expressed as the percentage of fluorescence compared with the control.

2.4. Determination of intracellular accumulation of DOX and Rho123

HepG2 cells were pre-incubated with or without 100 μM bile acids for 60 min, and cells were then incubated with or without 3 μM DOX in the presence or absence of 100 μM bile acids for 24 h. After the treatment, a portion of these cells were used to determine DOX, and the remaining cells were cultivated in fresh medium for 24 h. The latter cells were incubated with 3 μM Rho123 for 30 min at 37 °C. These cells were subsequently washed with phosphate-buffered saline (PBS, pH 7.4), and intracellular DOX and Rho123 were extracted with 1 ml of ethanol. A portion of these cells was used to measure fluorescence intensity with Arvo 1420 (PerkinElmer, Waltham, MA) at 480 nm/535 nm (emission/excitation) for DOX and 480 nm/580 nm (emission/excitation) for Rho123. A stock solution (3 mM) of Rho123 was prepared by dissolving it in DMSO.

2.5. Polymerase chain reaction (PCR) assay of MDR1 mRNA

We determined MDR1 mRNA levels by semi-quantitative RT-PCR. After cells were treated, total RNA was isolated using TRIzol Reagent (Invitrogen Japan) according to the manufacturer's instructions. cDNA was then prepared by incubating 0.5–1.0 μg of RNA with random primers (12.5 ng, Invitrogen Japan), RNase inhibitor (RNaseOUT, 20 units, Invitrogen Japan), 0.5 mM deoxynucleotide (dNTPs, Promega, Madison, WI), and 100 units of RNA reverse transcriptase (ReverTra Ace, TOYOBO, Tokyo, Japan) in 20 μl of the reaction buffer according to the ReverTra Ace data sheet. Following inactivation of the enzyme by incubation at 99 °C for 5 min, semi-quantitative PCR was performed with Blend Taq DNA polymerase (TOYOBO) using Thermal Cycler PxE (Thermo Fisher Scientific, Waltham, MA). PCR primers for MDR1 and GAPDH were synthesized by Hokkaido System Science. A primer set of the MDR1 gene was as follows; forward: 5′–AAGCTTAGTACCAAAGAGGCTCTG-3′, reverse: 5′–GGCTAGAAAACAATAGTGAAAACAA-3′. A primer set of GAPDH gene was as follows; forward: 5′–ACCACAGTCCATGCCATCAC-3′, reverse: 5′–TCCACCACCCTGTTGCTGTA-3′. PCR products (10 μl) were electrophoresed on a 1.5% agarose gel and visualized with ultraviolet light after immersion in an ethidium bromide solution (1 μg/ml, Sigma Japan) for 15 min. Images were taken with the digital camera CoolPix 9500 (Nikon, Tokyo, Japan) equipped with a BPB-60 filter (Fujifilm Japan, Tokyo, Japan). Densitometric analysis was performed using Image J for Windows supplied by the National Institutes of Health (Bethesda, MD).

2.6. Western blotting of P-gp

Cells were solubilized in loading dye containing 125 mM Tris (pH6.8, Sigma Japan), 5% sodium dodecylsulfate (SDS, Sigma Japan), 40% urea (Sigma Japan), and 0.2 M dithiothreitol (Sigma Japan). Samples were isolated using SDS-polyacrylamide gel electrophoresis (10% gel) and transferred onto a Hybond ECL Nitrocellulose membrane (GE Healthcare Japan, Tokyo, Japan). After blocking with skim milk, the membrane was treated with primary antibodies as follows. P-gp was detected with the C219 anti-MDR1 P-gp mouse monoclonal antibody (GeneTex, Irvine, CA) as a primary antibody and horseradish-labeled goat anti-mouse IgG2a antibody (Santa Cruz Biotechnology, Santa Cruz, CA) as a secondary antibody. The specific immunoreactive band of P-gp was detected using Immobilon Western Chemiluminescent HRP (Merck Japan, Tokyo, Japan) and a luminescence imager (LightCapture II, ATTO, Tokyo, Japan). Densitometric analysis was performed using Image J. GAPDH (Sigma Japan) was also detected as an internal standard protein using the anti-GAPDH antibody (Sigma Japan).

Cellular protein concentrations were determined using a DC protein assay kit (Bio-Rad Laboratories, Hercules, CA).

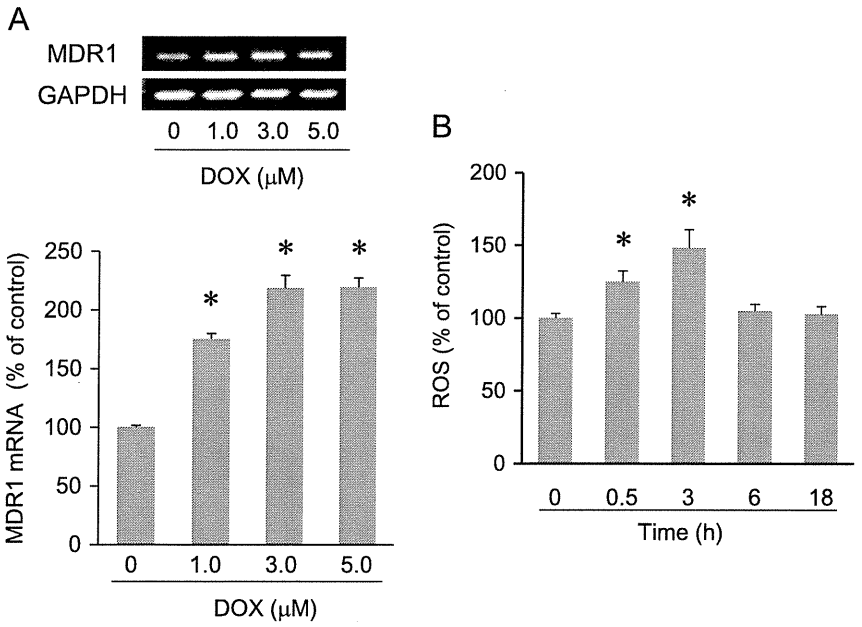

Fig. 1. Elevation in MDR1 gene expression and reactive oxygen species levels by DOX in HepG2 cells. (A) Cells were exposed to 1, 3, and 5 μM DOX or vehicle for 24 h, and RT-PCR was then conducted. Upper photographs are typical of agarose gel electrophoresis of RT-PCR products. Column graph data represent the relative expression level of MDR1 mRNA against GAPDH. (B) Cells were exposed to 3 μM DOX for the indicated periods and intracellular reactive oxygen species levels was determined as described in the Materials and Methods. Column graph data are expressed as the mean ± S.D. ($n=3$). *$P<0.05$, significantly different from the control.

2.7. Statistical analysis

Data are expressed as the mean ± S.D. Significance was determined by a one-way analysis of variance (ANOVA) and Holm's multiple-comparison test. $P<0.05$ was considered significant. All statistical analyses were performed using R Commander Plug-in for the EZR (Easy *R*) Package (RcmdrPlugin.EZR) (Kanda 2013).

3. Results

3.1. Increase in intracellular levels of MDR1 mRNA and reactive oxygen species by DOX in HepG2 cells and inhibition by NAC

The properties of DOX for the induction of MDR1 mRNA and reactive oxygen species levels in HepG2 cells were shown in Fig. 1A. MDR1 mRNA was induced in a dose-dependent manner after exposure to DOX for 24 h. However, our preliminary experiments indicated that this induction was not observed when cells were exposed to 3 μM DOX for 6 h (data not shown). When cells were continuously exposed to DOX (3 μM), intracellular reactive oxygen species levels increased in the early period, but returned to control levels within 6 h (Fig. 1B). To ascertain whether the elevation in MDR1 mRNA levels induced by DOX was dependent on the increase in reactive oxygen species levels, we examined the effect of NAC, an antioxidant and radical scavenger (Cotter et al., 2007). As shown in Fig. 2, the inductive effects of DOX (3 μM) on MDR1 mRNA and reactive oxygen species levels were significantly suppressed by NAC (0.5 mM). These results indicated that the induction of MDR1 mRNA by DOX depended on an elevation in intracellular reactive oxygen species levels in HepG2 cells treated with DOX.

3.2. Inhibitory effect of UDCA on DOX-induced elevations in MDR1 mRNA, P-gp, and reactive oxygen species levels in HepG2 cells

To investigate the inhibitory effect of UDCA on the DOX-induced overexpression of MDR1 mRNA and P-gp in HepG2 cells, cells were treated with 100 μM UDCA, a concentration that was shown to have anti-oxidative effects in our (Arisawa et al., 2009) and other previous studies (Mitsuyoshi et al., 1999; Rajesh et al., 2005; Okada et al., 2008).

DOX (3 μM) increased the expression of P-gp, as previously reported by Hu et al. (1995), and MDR1 mRNA in HepG2 cells. Although UDCA inhibited the DOX-induced elevation in MDR1 mRNA and P-gp levels, this dosage of UDCA itself did not influence the constitutive expression of MDR1 mRNA or P-gp (Fig. 3A–C). These results clearly demonstrated that UDCA inhibited the induction of P-gp and MDR1 gene expression by DOX in HepG2 cells.

We then investigated its effects on DOX-induced reactive oxygen species levels. As shown in Fig. 3D, UDCA inhibited the DOX-induced elevation in reactive oxygen species levels. A slight increase in reactive oxygen species levels was observed by UDCA alone.

3.3. Effects of UDCA on the intracellular accumulation of DOX and Rho123

To evaluate the transport function of DOX-induced *P*-gp and the effects of UDCA on this function, we examined the intracellular accumulation of DOX in HepG2 cells after combined exposure. As shown in Fig. 4A, UDCA increased the intracellular concentration of DOX after exposure for 24 h, while the combined exposure for 1 h failed to influence the intracellular accumulation of DOX. These results suggested that UDCA may have indirectly increased the accumulation of DOX after 24 h of exposure by inhibiting P-gp overexpression in the plasma membrane, as seen in Fig. 3A and C.

To functionally evaluate the effect of UDCA on P-gp levels, we investigated the intracellular accumulation of Rho123 after the treatment with DOX and UDCA for 24 h. As shown in Fig. 4B, UDCA by itself did not influence the uptake of Rho123. Rho123 levels were significant lower in cells pretreated with DOX than in untreated control cells. On the other hand, the accumulation of Rho123 was higher in cells pre-treated with both UDCA and DOX than in cells pre-treated with DOX alone.

These results suggested that UDCA inhibited the DOX-induced up-regulation of P-gp, which subsequently increased the intracellular accumulation of DOX and recovery of the accumulation of Rho123.

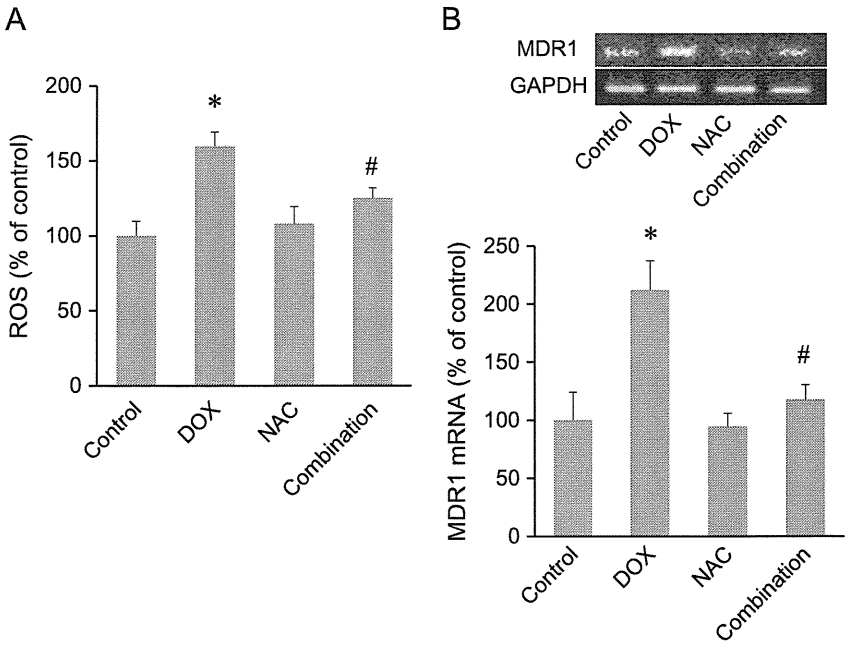

Fig. 2. Inhibition of DOX-induced increases in reactive oxygen species and MDR1 gene expression by NAC. Cells were pre-treated with 0.5 mM NAC for 1 h and then exposed to 3 μM DOX in the presence of NAC for 24 h. Reactive oxygen species measurements (A) and RT-PCR (B) were then conducted. Intracellular reactive oxygen species levels were determined using the fluorogenic dye CDCFH. Upper photographs are typical of agarose gel electrophoresis of RT-PCR products. Column graph data represent the relative expression levels of MDR1 mRNA against GAPDH. Column graph data are expressed as the mean ± S.D. ($n=3$). $^{*}P<0.05$, significantly different from the control. $^{\#}P<0.05$, significantly different from the DOX group.

3.4. Effects of CDCA, DCA, and LCA on P-gp, Rho123, and reactive oxygen species levels

We examined the effects of CDCA, DCA, and LCA to investigate if other bile acids also possessed properties similar to UDCA. As shown in Fig. 5A, CDCA (100 μM) partially inhibited the DOX-induced elevation in P-gp levels, while CDCA by itself did not affect P-gp levels. CDCA clearly inhibited the DOX-induced increase in reactive oxygen species levels (Fig. 7A), and also significantly reversed the DOX-induced reduction in intracellular Rho123 (Fig. 6A).

DCA (100 μM) did not affect DOX-induced P-gp overexpression (Fig. 5B), and had no effect on the intracellular accumulation of Rho123 (Fig. 6B) or DOX-induced elevation in intracellular reactive oxygen species levels (Fig. 7B).

The effect of LCA was investigated at 30 μM because 100 μM of LCA was cytocidal to HepG2 cells. As shown in Fig. 5C, LCA itself did not influence P-gp levels and did not influence the effect of DOX. LCA also had no effect on Rho123 uptake in cells treated without or with DOX (Fig. 6C). Although LCA increased reactive oxygen species levels by itself, it did not affect reactive oxygen species levels in combination with DOX (Fig. 7C). The reason for the lack of a correlation between LCA-induced reactive oxygen species and P-gp levels has yet to be established.

CDCA, DCA, and LCA reportedly stimulate PXR (Dussault et al., 2003) and MDR1 gene expression was previously shown to be stimulated by PXR (Geick et al., 2001). In the present study, the concentration of these bile acids may have been insufficient to induce an effect on HepG2 cells.

4. Discussion

In the natural course of chronic hepatitis C, most cases progress to liver cirrhosis, complicated by hepatocellular carcinoma. The oral administration of UDCA (typically 600 mg/day) is an alternative therapy for chronic hepatitis C in interferon-intolerant patients or non-responders, and long-term treatment is expected to improve prognosis (Omata et al., 2007). DOX is frequently used as a chemotherapeutic agent in the case of transarterial chemoembolism for hepatocellular carcinoma (Tinkle and Haas-Kogan, 2012). However, it has been shown to induce the overexpression of P-gp and antitumor multidrug resistance.

In this study, we ascertained that DOX induced P-gp, accompanied by an increase in intracellular reactive oxygen species levels, and showed that UDCA inhibited the DOX-induced up-regulation of P-gp, which reversed the decreased uptake of Rho123 in HepG2 cells pre-exposed to DOX, whereas UDCA itself had no effect on P-gp levels or Rho123 uptake. Additionally, we examined the combined effects of DOX and UDCA on P-gp levels even in Hep3B human hepatoma cells, and demonstrated that UDCA prevented the DOX-induced overexpression of P-gp (data not shown). Based on these results, it was suggested that UDCA may prevent the overexpression of P-gp induced by DOX and other anthracyclines and may also suppress the acquisition of antitumor multidrug resistance in various hepatoma cells including primary hepatoma cells. Furthermore, the clinical application of UDCA to chemotherapy for hepatocellular carcinoma, e.g. pre-and co-administration with DOX in the case of transarterial chemoembolism, may prevent the induction of P-gp by DOX and efflux of DOX from carcinoma cells, resulting in increases in its therapeutic effect.

To date, UDCA has been shown to increase MDR1 mRNA levels in Caco-2 cells, but not in intestinal or LS174T cells (Becquemont et al., 2006). On the other hand, CDCA (100 μM) increased MDR1 mRNA levels in Madin Darby canine kidney cells (Kneuer et al., 2007). In this study, UDCA and CDCA did not affect the basal expression of P-gp in HepG2 cells, but antagonized the DOX-induced increase in P-gp expression. These results indicate that the effect of UDCA and CDCA on basal MDR1 gene expression may be dependent on the types of cells and tissues studied, and these bile acids may not influence the basal expression of the MDR1 gene in hepatocellular carcinoma cells.